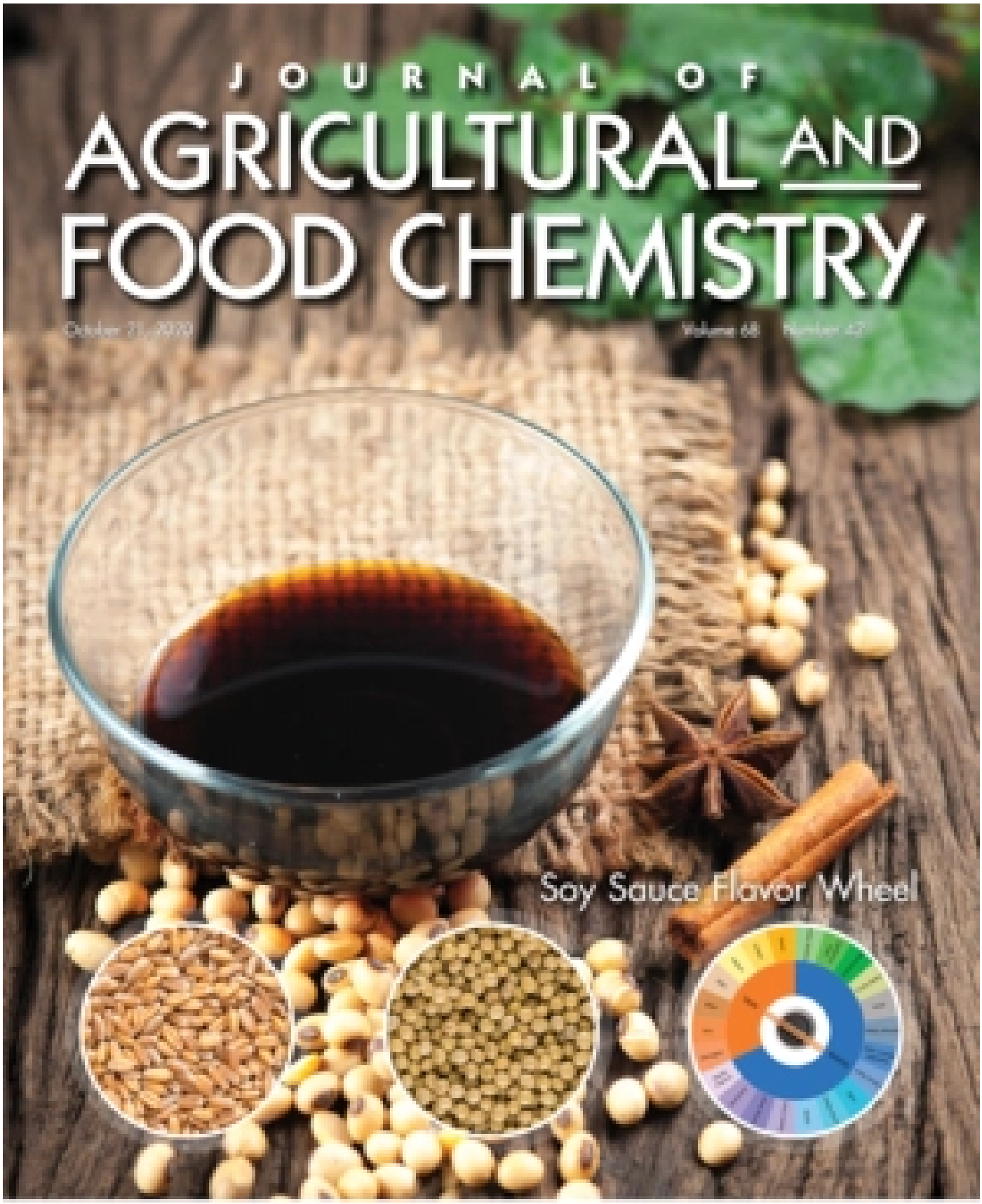

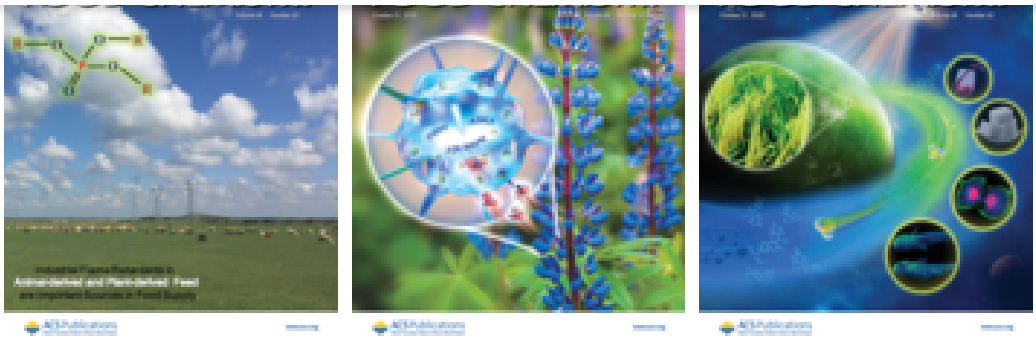

October 21, 2020
Volume 68, Issue 42
Pages 11595-11876

VIEW ALL ISSUES
ASAPs

About the Cover:

View the article.

Download Cover

In this issue:

Sort By: Page

REVIEWS

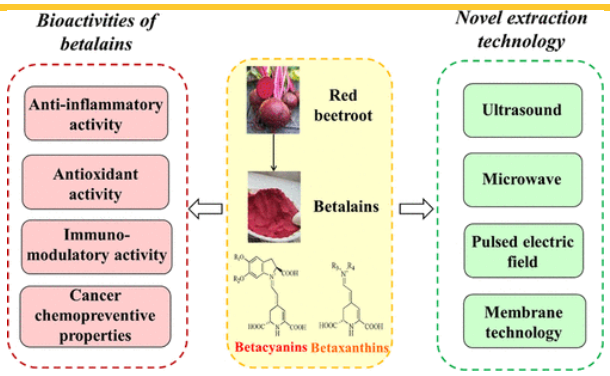

Red Beetroot Betalains: Perspectives on Extraction, Processing, and Potential Health Benefits

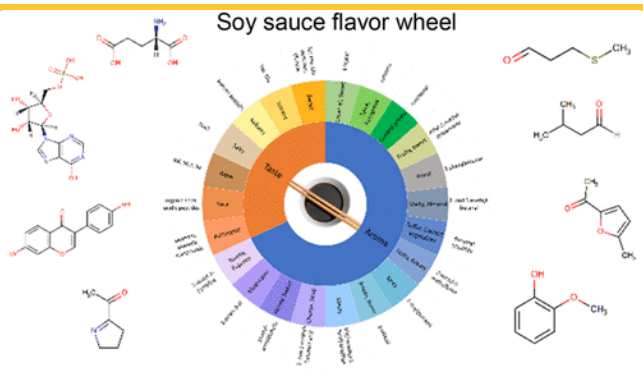

Chemical and Sensory Characteristics of Soy Sauce: A Review

Carmen Diez-Simon*, Charlotte Eichelsheim, Roland Mumm, and Robert D. Hall

Journal of Agricultural and Food Chemistry 2020, 68, 42, 11612-11630 **(Review)**
Publication Date (Web): September 3, 2020

Abstract Full text PDF

ABSTRACT

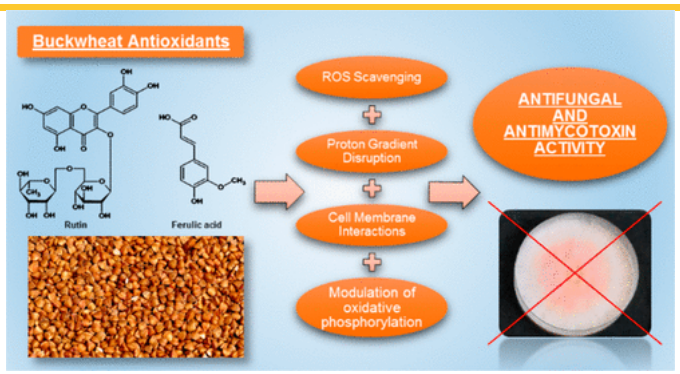

Buckwheat Secondary Metabolites: Potential Antifungal Agents

Daniel Koval*, Milada Plocková, Jan Kyselka, Pavel Skřivan, Marcela Sluková, and Šárka Horáčková

Journal of Agricultural and Food Chemistry 2020, 68, 42, 11631-11643 **(Review)**
Publication Date (Web): September 28, 2020

Abstract Full text PDF

ABSTRACT

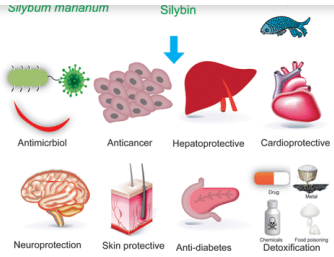

Health Benefits of *Silybum marianum*: Phytochemistry, Pharmacology, and Applications

Xin Wang, Zhen Zhang, and Shuai-Cheng Wu*

Journal of Agricultural and Food Chemistry 2020, 68, 42, 11644-11664 **(Review)**
Publication Date (Web): October 12, 2020

Abstract Full text PDF

ABSTRACT

AGRICULTURAL AND ENVIRONMENTAL CHEMISTRY

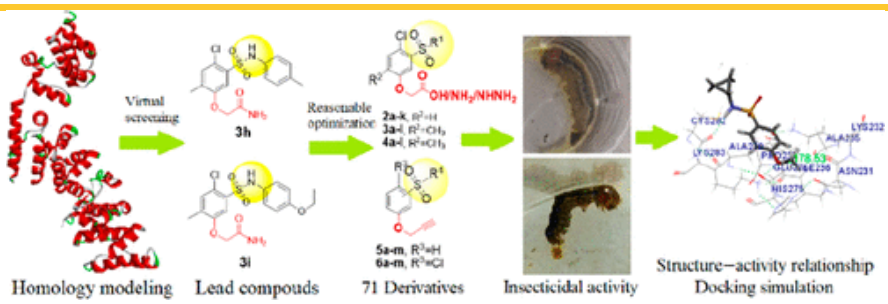

Synthesis and Insecticidal Activity Evaluation of Virtually Screened Phenylsulfonamides

Fangli Gang, Xiaoting Li, Chaofu Yang, Lijuan Han, Hao Qian, Shaopeng Wei, Wenjun Wu, and Jiwen Zhang*

Journal of Agricultural and Food Chemistry 2020, 68, 42, 11665-11671 **(Agricultural and Environmental Chemistry)**
Publication Date (Web): September 25, 2020

Abstract Full text PDF

ABSTRACT

Yue Deng, Rui Liu, Di Wu, Li Chen, Wenjun Zhang, Zikang Wang, Rujian He, Jinling Diao, and Zhiqiang Zhou*

Journal of Agricultural and Food Chemistry 2020, 68, 42, 11672-11683 **(Agricultural and Environmental Chemistry)**
Publication Date (Web): September 29, 2020

Abstract Full text PDF

ABSTRACT

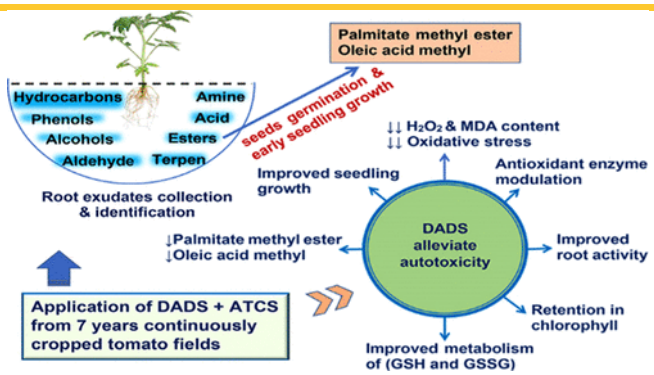

Garlic Allelochemical Diallyl Disulfide Alleviates Autotoxicity in the Root Exudates Caused by Long-Term Continuous Cropping of Tomato

Fang Cheng, Muhammad Ali, Ce Liu, Rui Deng, and Zhihui Cheng*

Journal of Agricultural and Food Chemistry 2020, 68, 42, 11684-11693 **(Agricultural and Environmental Chemistry)**
Publication Date (Web): September 29, 2020

Abstract Full text PDF

ABSTRACT

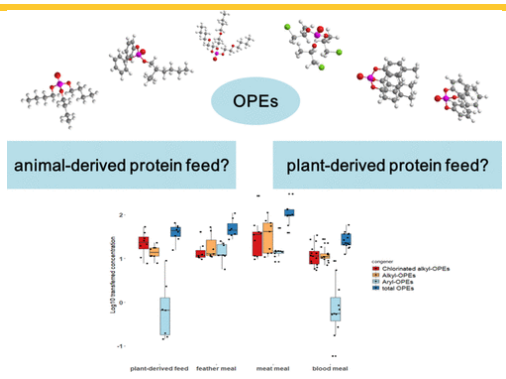

Animal-Derived and Plant-Derived Protein Supplement Feeds Are Important Sources of Organophosphate Esters in the Food Supply

Nannan Zhao, Jie Fu, Yifei Liu, Peilong Wang, Xiaoou Su, and Xiaomin Li*

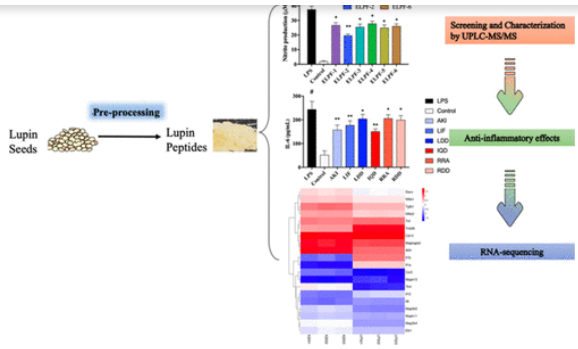

Peptides from Extruded Lupin (*Lupinus albus* L.) Regulate Inflammatory Activity via the p38 MAPK Signal Transduction Pathway in RAW 264.7 Cells

Yue Gao, Xuna Zhang, Guixing Ren, Caie Wu, Peiyou Qin*, and Yang Yao*

Journal of Agricultural and Food Chemistry 2020, 68, 42, 11702-11709 **(Bioactive Constituents, Metabolites, and Functions)**
Publication Date (Web): September 1, 2020

Abstract Full text PDF

ABSTRACT

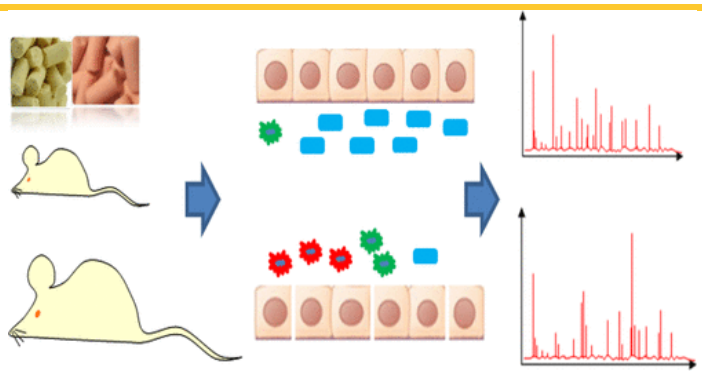

High-Fat Proteins Drive Dynamic Changes in Gut Microbiota, Hepatic Metabolome, and Endotoxemia-TLR-4-NFκB-Mediated Inflammation in Mice

Muhammad Ijaz Ahmad, Muhammad Umair Ijaz, Muzhair Hussain, Ijaz ul Haq, Di Zhao, and Chunbao Li*

Journal of Agricultural and Food Chemistry 2020, 68, 42, 11710-11725 **(Bioactive Constituents, Metabolites, and Functions)**
Publication Date (Web): October 9, 2020

Abstract Full text PDF

ABSTRACT

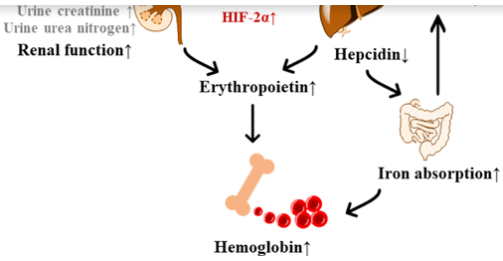

Collagen Hydrolysate Corrects Anemia in Chronic Kidney Disease via Anti-Inflammatory Renoprotection and HIF-2α-Dependent Erythropoietin and Hepcidin Regulation

Suqin Zhu, Lingyu Wu, Jiayou Zhang, Yu Miao, Yuanhui Zhao, Mingyong Zeng, Duo Li, and Haohao Wu*

Journal of Agricultural and Food Chemistry 2020, 68, 42, 11726-11734 **(Bioactive Constituents, Metabolites, and Functions)**
Publication Date (Web): September 27, 2020

Abstract Full text PDF

ABSTRACT

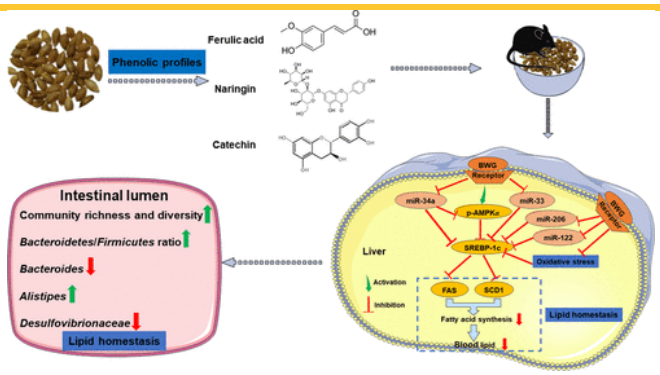

Highland Barley Whole Grain (*Hordeum vulgare L.*) Ameliorates Hyperlipidemia by Modulating Cecal Microbiota, miRNAs, and AMPK Pathways in Leptin Receptor-Deficient db/db Mice

Na Deng, Ziqian He, Ruixue Guo, Bisheng Zheng*, Tong Li, and Rui Hai Liu*

Journal of Agricultural and Food Chemistry 2020, 68, 42, 11735-11746 **(Bioactive Constituents, Metabolites, and Functions)**
Publication Date (Web): September 27, 2020

Abstract Full text PDF

ABSTRACT

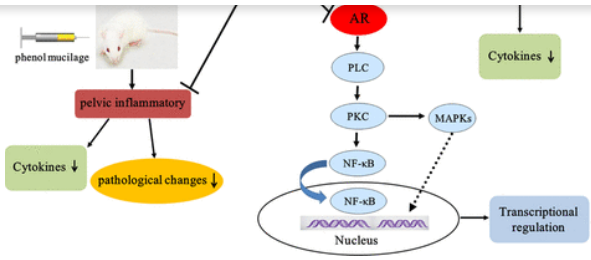

Aldose Reductase Inhibitor Engeletin Suppresses Pelvic Inflammatory Disease by Blocking the Phospholipase C/Protein Kinase C-Dependent/NF-κB and MAPK Cascades

Canmao Wang, Lei La, Haixing Feng, Qin Yang, Fuling Wu, Chunxia Wang, Jiangjie Wu, Lianbing Hou*, Chuqi Hou*, and Wenqin Liu*

Journal of Agricultural and Food Chemistry 2020, 68, 42, 11747-11757 **(Bioactive Constituents, Metabolites, and Functions)**
Publication Date (Web): October 13, 2020

Abstract Full text PDF

ABSTRACT

BIOTECHNOLOGY AND BIOLOGICAL TRANSFORMATIONS

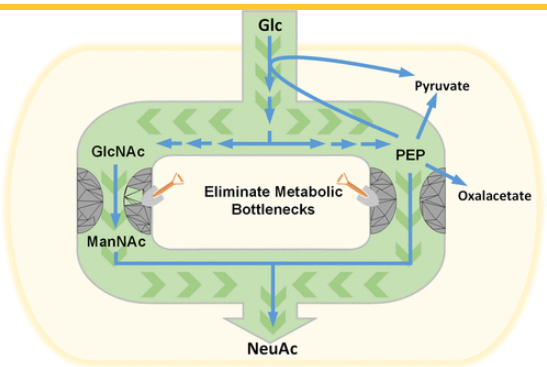

Exploring Amino Sugar and Phosphoenolpyruvate Metabolism to Improve *Escherichia coli N*-Acetylneuraminic Acid Production

Qingxiao Pang, Hao Han, Ya Xu, Xiaoqin Liu, Qingsheng Qi*, and Qian Wang*

Journal of Agricultural and Food Chemistry 2020, 68, 42, 11758-11764 **(Biotechnology and Biological Transformations)**
Publication Date (Web): September 22, 2020

Abstract Full text PDF

ABSTRACT

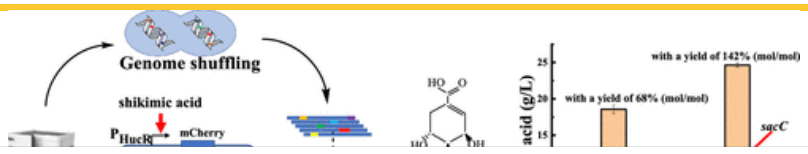

Fu-Xing Niu, Xin He, Yuan-Bin Huang, and Jian-Zhong Liu*

Journal of Agricultural and Food Chemistry 2020, 68, 42, 11765-11773 **(Biotechnology and Biological Transformations)**
Publication Date (Web): October 8, 2020

Abstract Full text PDF

ABSTRACT

CHEMISTRY AND BIOLOGY OF AROMA AND TASTE

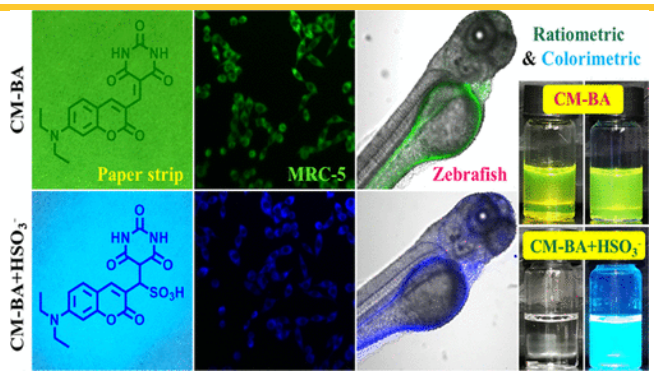

Reaction-Based Ratiometric and Colorimetric Chemosensor for Bioimaging of Biosulfite in Live Cells, Zebrafish, and Food Samples

Xiaojun He, Wei Xu, Feng Ding, Chuchu Xu, Yahui Li, Hong Chen*, and Jianliang Shen*

Journal of Agricultural and Food Chemistry 2020, 68, 42, 11774-11781 **(Chemistry and Biology of Aroma and Taste)**
Publication Date (Web): September 4, 2020

Abstract Full text PDF

ABSTRACT

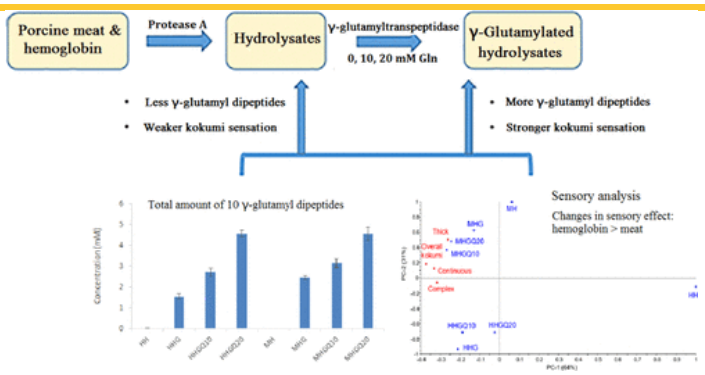

Production of Taste Enhancers from Protein Hydrolysates of Porcine Hemoglobin and Meat Using *Bacillus amyloliquefaciens* γ-Glutamyltranspeptidase

Qian Li, Jing Liu, Cristian De Gobba, Longteng Zhang, Wender L. P. Bredie, and René Lametsch*

FOOD AND BEVERAGE CHEMISTRY/BIOCHEMISTRY

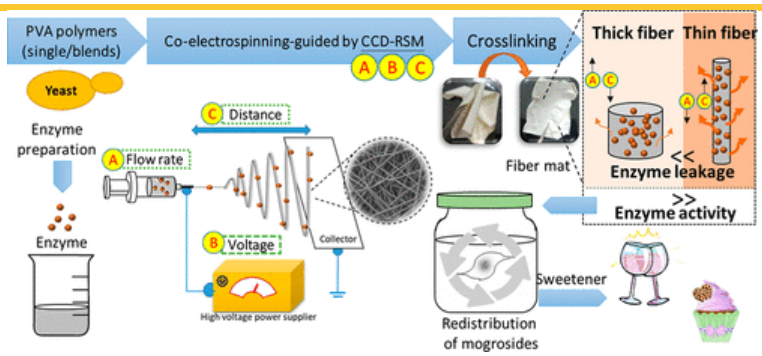

Encapsulation of β-Glucosidase within PVA Fibers by CCD-RSM-Guided Coelectrospinning: A Novel Approach for Specific Mogroside Sweetener Production

Virly, Chun-Hui Chiu, Tsan-Yu Tsai, Yi-Cheun Yeh, and Reuben Wang*

Journal of Agricultural and Food Chemistry 2020, 68, 42, 11790-11801 **(Food and Beverage Chemistry/Biochemistry)**
Publication Date (Web): September 29, 2020

Abstract Full text PDF

ABSTRACT

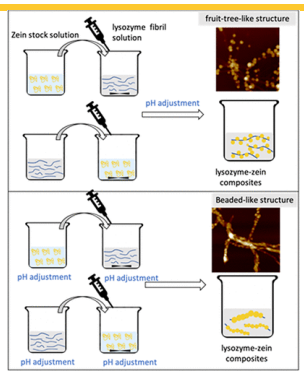

Fabrication of Composite Structures of Lysozyme Fibril–Zein using Antisolvent Precipitation: Effects of Blending and pH Adjustment Sequences

Jingru Song, Cuixia Sun, Yanwei Xiang, Yun Xie, Analucia Mata, and Yapeng Fang*

Journal of Agricultural and Food Chemistry 2020, 68, 42, 11802-11809 **(Food and Beverage Chemistry/Biochemistry)**
Publication Date (Web): September 29, 2020

Abstract Full text PDF

ABSTRACT

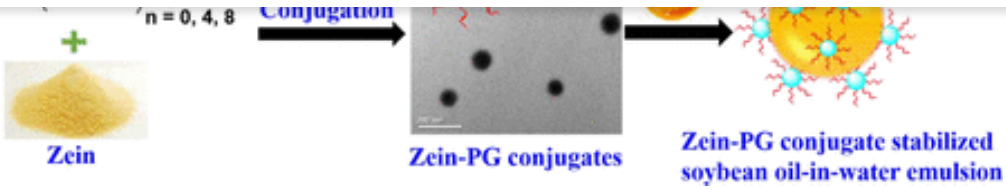

Zein-Polyglycerol Conjugates with Enhanced Water Solubility and Stabilization of High Oil Loading Emulsion

Shuangshuang Huang, Junbo He*, Lijuan Han, Hong Lin, Gang Liu, and Weinong Zhang*

Journal of Agricultural and Food Chemistry 2020, 68, 42, 11810-11816 **(Food and Beverage Chemistry/Biochemistry)**
Publication Date (Web): September 29, 2020

Abstract Full text PDF

ABSTRACT

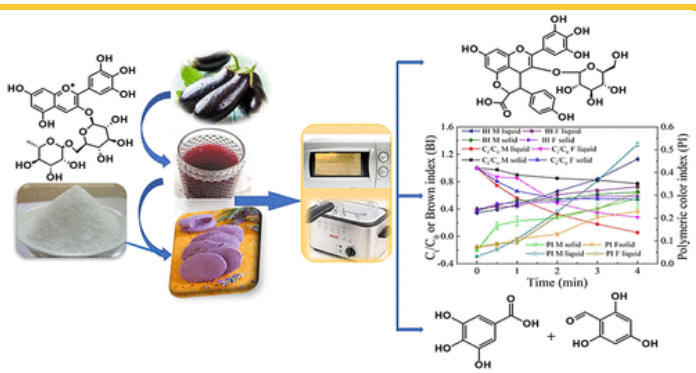

Degradation Kinetics of Anthocyanins from Purple Eggplant in a Fortified Food Model System during Microwave and Frying Treatments

Yanfei Zhang, Zeyuan Deng*, Hongyan Li, Liufeng Zheng, Rong Liu, and Bing Zhang*

Journal of Agricultural and Food Chemistry 2020, 68, 42, 11817-11828 **(Food and Beverage Chemistry/Biochemistry)**
Publication Date (Web): September 25, 2020

Abstract Full text PDF

ABSTRACT

FOOD SAFETY AND TOXICOLOGY

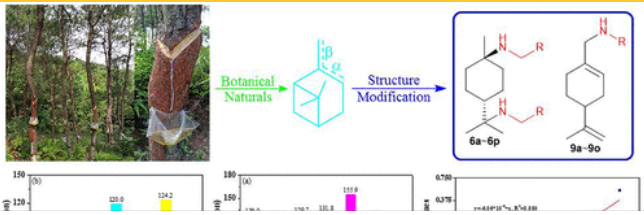

Shichao Xu, Xiaojing Zeng, Songlin Dai, Jing Wang, Yuxiang Chen, Jie Song*, Yunfei Shi, Xian Cheng, Shengliang Liao*, and Zhendong Zhao*

Journal of Agricultural and Food Chemistry 2020, 68, 42, 11829-11838 **(Food Safety and Toxicology)**
Publication Date (Web): September 25, 2020

Abstract Full text PDF

ABSTRACT

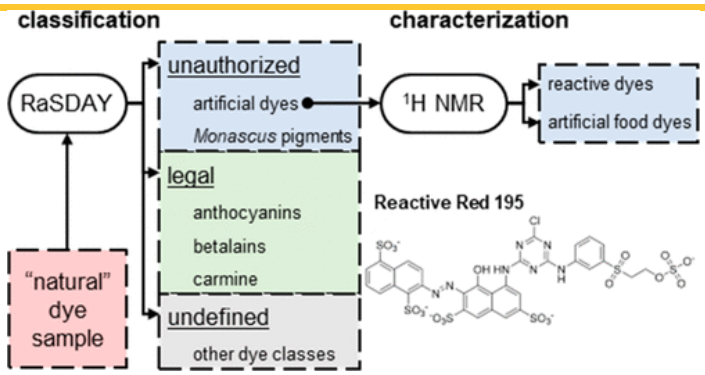

Rapid UV/Vis Spectroscopic Dye Authentication Assay for the Determination and Classification of Reactive Dyes, *Monascus* Pigments, and Natural Dyes in Coloring Foodstuff

Edwin Januschewski, Greta Bischof, Binh Nguyen Thanh, Pia Bergmann, Gerold Jerz, Peter Winterhalter, Volker Heinz, and Andreas Juadjur*

Journal of Agricultural and Food Chemistry 2020, 68, 42, 11839-11845 **(Food Safety and Toxicology)**
Publication Date (Web): October 9, 2020

Abstract Full text PDF

ABSTRACT

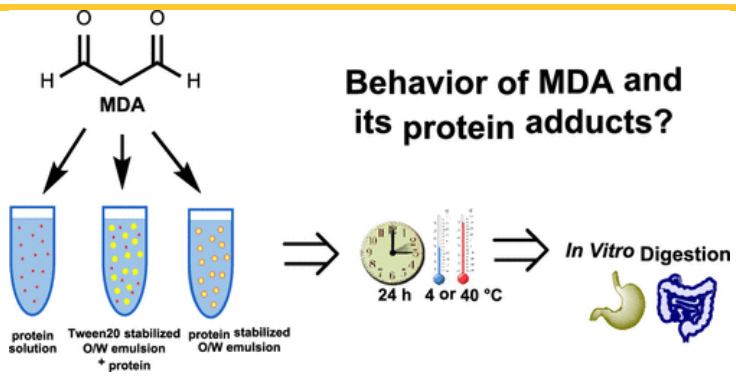

Behavior of Malondialdehyde and Its Whey Protein Adducts during *In Vitro* Simulated Gastrointestinal Digestion

Angelique Vandemoortele, Pinar Babat, Mariam Yakubu, and Bruno De Meulenaer*

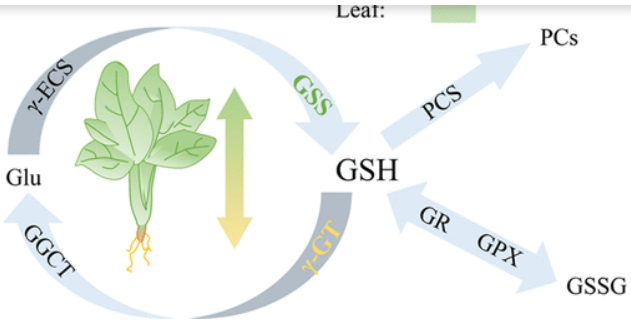

Decisive Enzymes and Prediction Models for the Glutathione Content in Spinach (*Spinacia oleracea L.*) Exposed to Cadmium

Ya Gao, Haipu Li*, Yang Song, Fenglin Zhang, Yi Lu, Fangyuan Peng, and Zhaoguang Yang*

Journal of Agricultural and Food Chemistry 2020, 68, 42, 11855-11862 **(Food Safety and Toxicology)**
Publication Date (Web): September 28, 2020

Abstract Full text PDF

ABSTRACT

OMICS TECHNOLOGIES APPLIED TO AGRICULTURE AND FOOD

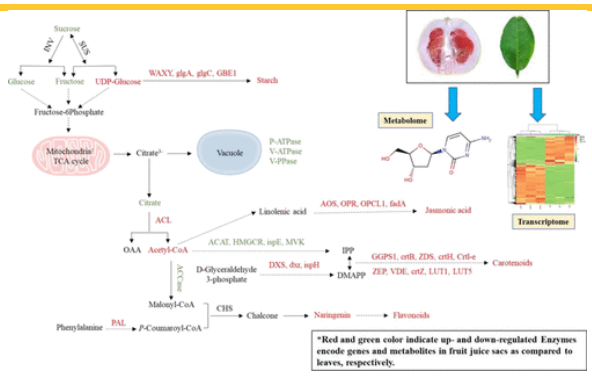

Multiomic Analysis Elucidates the Reasons Underlying the Differential Metabolite Accumulation in Citrus Mature Leaves and Fruit Juice Sacs

Ling-Xia Guo, Syed Bilal Hussain, Alisdair R. Fernie, Yong-Zhong Liu*, Min Yan, Huan Chen, and Shariq Mahmood Alam

Journal of Agricultural and Food Chemistry 2020, 68, 42, 11863-11874 **(Omics Technologies Applied to Agriculture and Food)**
Publication Date (Web): October 8, 2020

Abstract Full text PDF

ABSTRACT

ADDITIONS AND CORRECTIONS

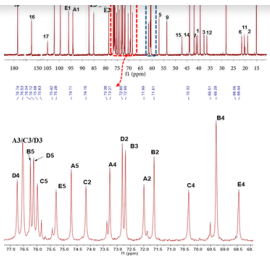

Correction to RQ3, A Natural Rebaudioside D Isomer, Was Obtained from Glucosylation of Rebaudioside A Catalyzed by the CGTase Toruzyme 3.0 L

Qingbin Guo, Tongtong Zhang, Nifei Wang, Yongmei Xia*, Zhuoyu Zhou, Jian-rong Wang, and Xuefeng Mei

Journal of Agricultural and Food Chemistry 2020, 68, 42, 11875-11876 **(Addition/Correction)**
Publication Date (Web): October 7, 2020

Full text PDF

MASTHEADS

Issue Editorial Masthead

Journal of Agricultural and Food Chemistry 2020, 68, 42, XXX-XXX **(Article)**
Publication Date (Web): October 21, 2020

PDF

Issue Publication Information

Journal of Agricultural and Food Chemistry 2020, 68, 42, XXX-XXX **(Article)**
Publication Date (Web): October 21, 2020

PDF

JOURNAL OF AGRICULTURAL AND FOOD CHEMISTRY

Editors & Editorial Board

Editor-in-Chief

Thomas F. Hofmann
Technische Universität München
Germany
E-mail: hofmann-office@jafc.acs.org

Current Issue Editorial Masthead

View the Masthead in Current Issue

Associate Editors

Sonia de Pascual-Teresa
ICTAN-CSIC
Spain
E-mail: depascualteresa-office@jafc.acs.org

Yolanda Gogorcena
CSIC
Spain
E-mail: gogorcena-office@jafc.acs.org

Cathleen J. Hapeman
US Department of Agriculture
United States
E-mail: hapeman-office@jafc.acs.org

Qing X. Li
University of Hawai'i at Manoa
United States
E-mail: li-office@jafc.acs.org

John Munafo
University of Tennessee
United States
E-mail: munafo-office@jafc.acs.org

Shaoping Nie
Nanchang University
China
E-mail: nie-office@jafc.acs.org

Min-Hsiung Pan

Shengmin Sang
North Carolina A&T State University
United States
E-mail: sang-office@jafc.acs.org

Katharina Scherf
Karlsruhe Institute of Technology
Germany
E-mail: scherf-office@jafc.acs.org

Veronika Somoza
University of Vienna
Austria
E-mail: somoza-office@jafc.acs.org

Birte Svensson
Technical University of Denmark
Denmark
E-mail: svensson-office@jafc.acs.org

Liangli (Lucy) Yu
University of Maryland
United States
E-mail: yu-office@jafc.acs.org

Holger Zorn
Justus-Liebig-Universitat Giessen
Germany
E-mail: zorn-office@jafc.acs.org

American Chemical Society
United Kingdom
E-mail: wking@acs-i.org

Editorial Advisory Board

1155 Sixteenth Street N.W.
Washington, DC 20036

JOURNAL OF AGRICULTURAL AND FOOD CHEMISTRY

pubs.acs.org/JAFC Article

Encapsulation of β-Glucosidase within PVA Fibers by CCD-RSM-Guided Coelectrospinning: A Novel Approach for Specific Mogroside Sweetener Production

Virly,[▽] Chun-Hui Chiu,[▽] Tsan-Yu Tsai, Yi-Cheun Yeh, and Reuben Wang*

Cite This: J. Agric. Food Chem. 2020, 68, 11790−11801 Read Online

ACCESS | Metrics & More | Article Recommendations | Supporting Information

ABSTRACT: Siamenoside I is a rare mogroside in *Siraitia grosvenorii* Swingle and has become one of the target ingredients in natural sweetener production. However, the complex structure of siamenoside I has hindered its production in various ways. Here, a yeast cell that produces a specific β-glucosidase for siamenoside I conversion from mogroside V was constructed, and the enzymes were coelectrospun with poly(vinyl alcohol) followed by phenylboronic acid cross-linking to provide potential usage in the batch production process of Siamenoside I. A central composite design (CCD)-response surface methodology (RSM) was used to find the optimum coelectrospinning parameters. The pH stability and sodium dodecyl sulfate tolerance increased for the entrapped enzymes, and positive correlations between the fiber diameter and enzymatic activity were confirmed. The batch process showed an average siamenoside I production rate of 118 ± 0.08 mg L^{-1} h^{-1} per gram of fiber. This is the first research article showing specific siamenoside I production on enzyme-loaded electrospun fibers.

KEYWORDS: *siamenoside I, β-glucosidase, poly(vinyl alcohol), coelectrospinning, CCD-RSM*

INTRODUCTION

Monk fruit or *Luo Han Guo* in Chinese (*Siraitia grosvenorii* Swingle) is one type of Curcubitaceae fruit found in the southern part of China. It has been used for thousands of years as a traditional Chinese medicine in treating sore throat, high blood pressure, and constipation.[1] The monk fruit extract contains saponin mixtures called mogrosides (MGs) with high sweet intensities[2] and is considered to be a generally recognized as safe (GRAS) ingredient according to the U.S. FDA.[3] Each mogroside molecule comprises one aglycone called mogrol and is attached to several different glucose moieties at its C-3 and C-24 sites. For example, the most abundant mogroside in the fruit extract, mogroside V (MG V), has two and three glucose moieties bound to the C-3 and C-24 sites, respectively (Figure 1A). Meanwhile, both mogroside IV (MG IV) and siamenoside I (S I) have four glucose moieties attached to the mogrol in different patterns.[4−6]

Although there are several kinds of MGs in monk fruit, namely, MG VI, MG V, 11-oxo-MG V, MG IV, S I, MG III E, MG II, and MG I, few kinds are sweet.[2,5] For example, some studies showed that the sweetest mogroside, S I, is 563 times sweeter than 5% sucrose solution, although this compound accounts for less than 5% of total MGs.[2,7,8] Moreover, unlike other types of sweet MGs with sweet profiles varying from that of sucrose,[9] the sweetness characteristics of S I were more similar to those of sucrose, without any aftertaste.[10]

Several attempts have been made to develop procedures for obtaining S I, and most of them have focused on the transformation of MG V into S I. The reason is because MG V accounts for 60% of the total MGs in the fruit without enrichment,[8] and if a 100% conversion rate could be reached, large amounts of S I could be obtained. However, methods including acid hydrolysis, enzymatic treatment, and in vivo digestion all have shown little effect on generating S I from MG V due to low specificity, as the chemical structures of these two compounds only differ by one glucose moiety, where MG V has one additional glucose on the C-3 position of S I, with a β (1 → 6) linkage (Figure 1A).[2,11,12] Recently, the transformation of MG V using microbes has shed light on the specific production of S I from MG V. *Saccharomyces cerevisiae* BY4741 wild-type cells were able to produce β-glucosidase (*Sc*Exg1), which acts on peripheral glucose with (1 → 6)-β-D-glucosyl linkages at the C-3 and C-24 positions of MG V, generating S I and MG IV as intermediates and MG III E as the end product.[13] Additionally, the β-glucosidase produced by *Dekkera bruxellensis* (*Db*Exg1) alternatively acts only on the peripheral glucose of MG V with (1 → 6)-β-D-glucosyl linkages at the C-3 position, generating only S I from MG V.[14] To the best of our knowledge, to date, no studies have focused on using *Db*Exg1 in the redistribution of mogrosides for S I enrichment.

The high degree of substrate selectivity, energy efficiency, and cost-effectiveness of the enzyme as a biocatalyst have made it widely applied in various applications. Nevertheless, its vulnerability to structural changes caused by unconducive reaction conditions, including extreme pH, temperature, and

Received: April 21, 2020
Revised: August 6, 2020
Accepted: September 29, 2020
Published: September 29, 2020

https://dx.doi.org/10.1021/acs.jafc.0c02513
J. Agric. Food Chem. 2020, 68, 11790−11801

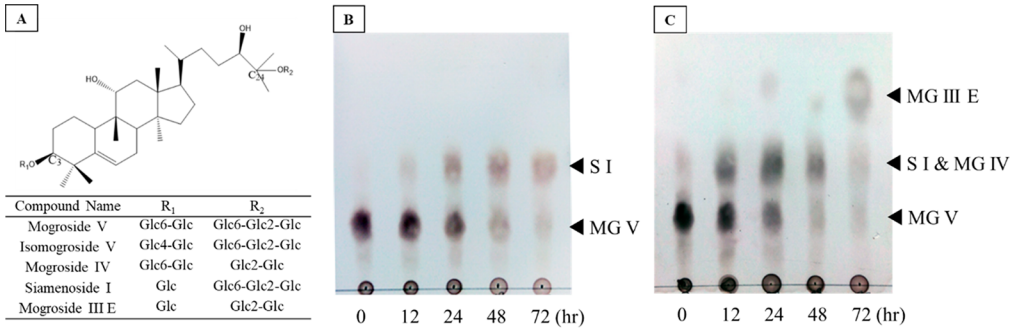

Compound Name	R_1	R_2
Mogroside V	Glc6-Glc	Glc6-Glc2-Glc
Isomogroside V	Glc4-Glc	Glc6-Glc2-Glc
Mogroside IV	Glc6-Glc	Glc2-Glc
Siamenoside I	Glc	Glc6-Glc2-Glc
Mogroside III E	Glc	Glc2-Glc

Figure 1. Mogrosides redistribution profiles analyzed by TLC. (A) The chemical structure of mogrosides. Mogrosides redistribution in (B) *S. cerevisiae* BY4741 *exg1*Δ*::DbEXG1* and (C) *S. cerevisiae* BY4741 WT.

the presence of disturbing chemical agents, limits its reusability and application on a larger scale and in a continuous production system.[15,16] To solve the aforementioned constraints of free-form enzymes, an enzyme immobilization technique can be performed.[17,18] Among all the enzyme immobilization techniques, entrapping enzymes in scaffolds has currently gained much attention.

Electrospinning is a method that uses an applied electric force to draw charged polymer solutions in the form of fibers toward a collector, resulting in fibers with high porosity and a high surface-to-volume ratio.[19,20] The coelectrospinning method is a process of combining two different materials and fabricating them into fibers in a single step, which allows minimum usage of chemicals and heat treatment.[21] Additionally, the high voltage applied during the coelectrospinning process has been suggested to have little effect on the tertiary structure of the enzymes.[22] Previously, several studies have demonstrated the suitability of this method in controlling enzyme release,[23] increasing the tolerance to extreme pH and temperature,[24] prolonging the storage stability,[25] increasing the reusability,[26,27] and enhancing the activities of the immobilized enzymes.[28]

In the present study, we endeavored to test the feasibility of S I production in a batch process in which fibers with specific enzymes were submerged in a flask containing MG V as the starting material. Poly(vinyl alcohol) (PVA) was chosen as supporting material of enzymes due to its high biocompatibility and nontoxigenic characteristics.[23] To achieve this aim, the produced enzyme/PVA fibers were first cross-linked to alter the hydrophilic nature of PVA. By using central composite design-response surface methodology (CCD-RSM), optimization of the electrospinning parameters (i.e., flow rate, applied voltage, and distance between spinneret and collector) was performed to generate a combination of parameters that produced fibers with the highest enzymatic activity as well as to study the relation of the activity to the fiber diameter. Additionally, the potential of the coelectrospinning method in addressing the problem of sustainable S I production was evidenced by demonstrating the reusability and robustness of the enzyme/PVA fibers. Finally, the S I production rate in this batch production process was calculated.

MATERIALS AND METHODS

Construction of Yeast Cells with *Db*Exg1 Secretion Activity. To create a yeast strain with stable *Db*Exg1 secretion activity, the gene responsible for the enzyme could be obtained from the *DbEXG1* expression vector using the PCR amplification method.[14] *S. cerevisiae* (BY4741 *exg1*Δ*::KanMX4*) lacking *URA3* was chosen as the host cell, allowing us to select successfully gene-transformed colonies harboring *DbEXG1* linked with *URA3* (*DbEXG1-URA3*), which would then appear on Ura^- plates. However, the source of *DbEXG1,* which originates from the *DbEXG1* expression vector, was not directly linked to *URA3*; instead, there was an antibiotic resistance gene (ampR) between *DbEXG1* and *URA3*. Because there were concerns about the presence of antibiotic-resistant genes in the food system, we deleted ampR in the *DbEXG1* expression vector before using it as a template for *DbEXG1-URA3* amplification. The deletion of ampR was performed by first applying the inverse PCR method with back-to-back primers to amplify part of the *DbEXG1* expression vector, followed by ligation of the linear product to form circular DNA. The circular DNA was then used as the template for amplification of the *DbEXG1-URA3* target gene for DNA transformation. During the strain construction process, we were able to replace the *exg1*Δ*::KanMX4* gene cassette in BY4741 *exg1*Δ cells with *DbEXG1-URA3* at the chromosomal level through indigenous homologous recombination pathways in yeast. These processes result in cells having exogenous *DbEXG1* and were indicated as *S. cerevisiae* BY 4741 *exg1*Δ*::DbEXG1* in this study. Figure S1 of the Supporting Information (SI) shows a conceptual schematic of the inverse PCR process for this study, whereas Table S1 and Figure S2A show the primers with the sequence used for obtaining *DbEXG1-URA3* genetic materials and transformation results, respectively.

Confirmation of Siamenoside I Conversion from Mogroside V in the Gene-Transformed Cells. The test of MG conversion to S I in newly constructed cells (*S. cerevisiae exg1*Δ*::DbEXG1*) begins with the inoculation of cells in yeast extract-peptone-dextrose (YPD)-MGs medium. The YPD-MGs medium was prepared by adding 0.5% (w/v) of a commercially available powder of monk fruit extracts containing 80% MG V (Huilin Biotech Co., Ltd., Xi'an city, China) into the YPD medium. The MG conversion was carried out aerobically at 30 °C for 0, 12, 24, 48, and 72 h on an orbital shaker (200 rpm). Samples of cell-free supernatant were obtained after centrifugation (6000*g*, 10 min, 4 °C). The MGs in the supernatants were then extracted using solid-phase extraction (SPE) cartridges manufactured by Cayman Chemical (C-18, 500 mg/6 mL, FineTech, Taichung, Taiwan). Pure methanol was first infused to activate the cartridge, followed by water to equilibrate the system before sample loading. The unbound impurities and the MGs were eluted using 45% methanol and pure methanol, respectively.

The eluted MGs were first concentrated via a rotary evaporator, and the concentrates were applied onto thin layer chromatography (TLC) silica gel 60 plates (Merck, Germany). The TLC plates were developed in a chamber loaded with the developing solvent containing butanol−acetic acid−water with a 5:4:1 (v/v/v) ratio at the lower phase. After the plate was fully permeated with the developing solvent, the remaining solvent on the plate was allowed to evaporate, and the plate was sprayed with 10% (v/v) H_2SO_4 to oxidize the mogrosides compound. The visualization of the results was performed after heating the plate on top of a dry incubator at 100 °C for 5 min.[14,29] The MG conversion profile of *S. cerevisiae* BY4741 WT served as a control, following the identical cell cultivation and analysis procedures mentioned above.

https://dx.doi.org/10.1021/acs.jafc.0c02513
J. Agric. Food Chem. 2020, 68, 11790−11801

Table 1. CCD of Electrospinning Parameters with Enzymatic Activity and Diameter Responses

		levels				
factors		$-\alpha$	-1	0	1	α
A: flow rate (mL/min)		0.003	0.004	0.006	0.008	0.009
B: voltage (kV)		12.2	12.5	13.0	13.5	13.8
C: distance (cm)		10.8	12.5	15.0	17.5	19.2
run	A: flow rate (mL/min)	B: voltage (kV)	C: distance (cm)		enzymatic activity (μU/mg)	diameter (nm)
1	0	0	0		213.57 ± 25.84	254
2	0	0	0		208.21 ± 26.67	267
3	0	0	0		209.04 ± 11.94	245
4	0	0	0		209.83 ± 33.64	240
5	1	1	−1		234.02 ± 22.04	310
6	0	0	$-\alpha$		226.30 ± 10.01	276
7	−1	1	−1		136.77 ± 15.7	273
8	α	0	0		243.65 ± 10.83	343
9	$-\alpha$	0	0		139.64 ± 3.18	262
10	0	$-\alpha$	0		160.52 ± 8.82	294
11	−1	1	1		136.77 ± 4.6	246
12	0	0	0		223.49 ± 9.54	227
13	−1	−1	1		47.07 ± 12.76	245
14	1	−1	−1		265.06 ± 24.49	351
15	1	−1	1		68.19 ± 6.41	258
16	0	0	0		201.47 ± 19.42	231
17	0	α	0		119.51 ± 4.23	276
18	1	1	1		91.71 ± 9.42	225
19	0	0	α		32.27 ± 1.68	179
20	−1	−1	−1		239.11 ± 42.24	294

Preparation of the Crude Extract of *Db*Exg1. To collect the extracellular protein *Db*Exg1, the supernatant from the culture of *S. cerevisiae exg1*Δ::*DbEXG1* cells, which were cultivated in YPD broth at 30 °C for 72 h with orbital shaking (200 rpm), was first collected by centrifugation (6000*g* for 10 min at 4 °C). These supernatants were frozen at −80 °C and lyophilized using a laboratory-scale freeze-dryer (Kingmech, Model FD4.5-8P-L, Taiwan). To increase the purity of the target protein, the dried supernatant in powder form was resuspended in distilled deionized water (DDW) (10% w/v) and loaded into a 12−14 kDa molecular weight cutoff (MWCO) ultrafiltration membrane, which was then dialyzed three times in DDW with a 1:100 ratio (v/v) at 4 °C for 6 h. The dialyzed suspension was then freeze-dried and kept at −80 °C before further usage.

***Db*Exg1/PVA (Enzyme/PVA) Fiber Fabrication and Cross-Linking.** The 8% (w/v) PVA (poly(vinyl alcohol); 99% hydrolyzed, M_W 85 000−124 000, Sigma-Aldrich Chemical Co., U.S.A.) solution in acetate buffer (20 mM at pH 5.0) was prepared in a water bath set at 80 °C with magnetic agitation for 3 h. After cooling to room temperature, the freeze-dried enzyme-enriched powder was mixed with the PVA solution with agitation to obtain a homogeneous mixture. The prepared mixtures were filled in a 5 mL Terumo syringe (23 G, 13 mm inside diameter) and delivered to the spinneret with the typical flow rate maintained at 0.006 mL/mins controlled by an infusion pump (New Era Pump Systems, Model NE-300, U.S.A.). The spinneret was connected to a high-voltage power supply (Falco, Model FES-HV30, Taiwan) with the applied voltage set at 13.0 kV. The horizontal distance between the tip of the spinneret and the baking paper-covered collector plate was fixed at 15.0 cm. The generated fibers were then stored inside a dry cabinet with 65% relative humidity at 22 °C for 24 h to allow the remaining solvent to evaporate before cross-linking.

The cross-linking of fibers was performed according to Nunes et al. with few modifications.[18] First, the fibers were dipped into a 1% (w/v) phenylboronic acid solution for 2 to 10 min according to different settings. Afterward, the fibers were immersed in citrate-phosphate buffer adjusted to pH 5.0 for 5 s to eliminate the remaining cross-linking solution and were then air-dried before further analysis.

Optimization of Electrospinning Parameters Using CCD-RSM. The main parameters in electrospinning include the flow rate, applied voltage, and distance between the spinneret and collector. These were optimized into a combination of parameters that produced fibers with the highest enzymatic activity. Additionally, the diameter of the produced fibers along with their relationship with enzymatic activity was studied.

First, we wanted to ensure that each of the testing parameters was within a reasonable range for electrospinning. Then, the five-level numbers for each parameter, including the center point, were set within this particular range. The five-level numbers, as well as their combinations of optimization experiments with other parameters, were set by central composite design (CCD) software (Design-Expert 12.0.0). According to this CCD tool, we only needed to include 14 sets of control factor (the three electrospinning parameters) experiments and 6 replicates of the center point to estimate the pure error sum of squares (Table 1). From this experimental design, the diameter of the fibers was set to be the response variable. Then, the data in the diameter of fibers were fitted into the quadratic model shown in eq 1:

$$Y = \beta_0 + \beta_1 X_1 + \beta_2 X_2 + \beta_3 X_3 + \beta_{12} X_1 X_2 + \beta_{13} X_1 X_3 + \beta_{23} X_2 X_3 + \beta_{11} {X_1}^2 + \beta_{22} {X_2}^2 + \beta_{33} {X_3}^2 \quad (1)$$

In addition, the enzymatic activity of fibers obtained from each parameter combination was fitted to the cubic model shown in eq 2:

$$Y = \beta_0 + \beta_1 X_1 + \beta_2 X_2 + \beta_3 X_3 + \beta_{12} X_1 X_2 + \beta_{13} X_1 X_3 + \beta_{23} X_2 X_3 + \beta_{11} {X_1}^2 + \beta_{22} {X_2}^2 + \beta_{33} {X_3}^2 + \beta_{123} X_1 X_2 X_3 + \beta_{112} X_1 X_1 X_2 + \beta_{122} X_1 X_2 X_2 \quad (2)$$

In eqs 1 and 2, Y is the response variable, β_0 is the interception coefficient, β_1, β_2, β_3, β_{12}, β_{13}, β_{23}, β_{11}, β_{22}, β_{33}, β_{123}, β_{112}, and β_{122} are the estimated coefficients of the equation, and X_1, X_2, and X_3 are the manipulated control factors representing the flow rate (A), applied

https://dx.doi.org/10.1021/acs.jafc.0c02513
J. Agric. Food Chem. 2020, 68, 11790−11801

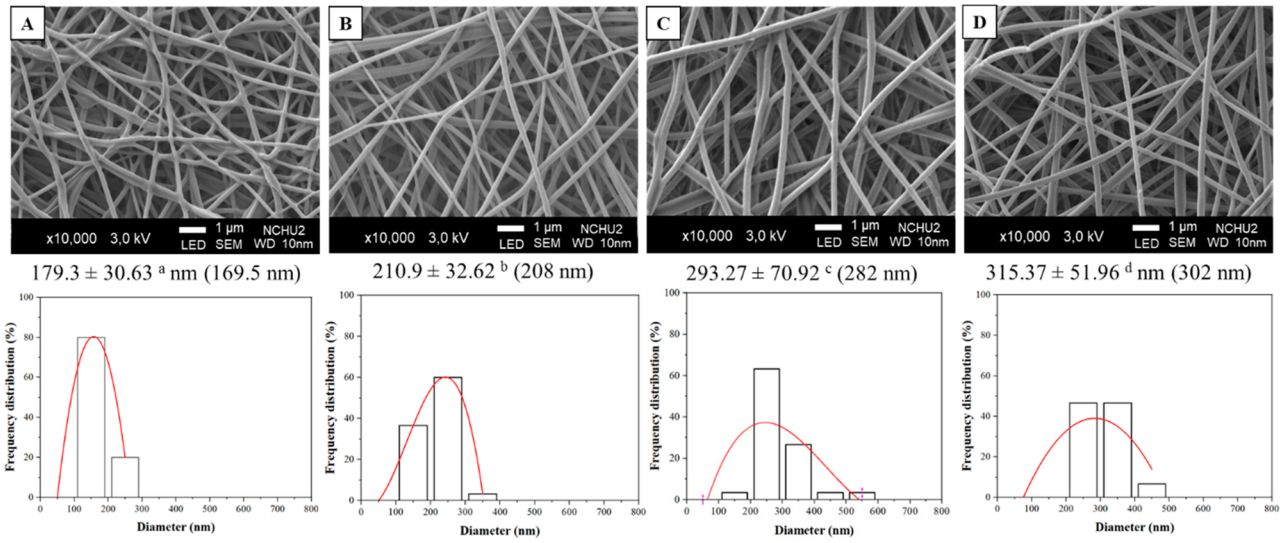

Figure 2. SEM micrographs of PVA electrospun fibers loaded with (A) 4%, (B) 5%, (C) 6%, and (D) 7% enzyme and their respective fiber diameters. Average values in diameters that do not share the same letter denote statistical significance ($p < 0.05$). The data were analyzed by one-way ANOVA followed by Duncan's multiple test. Additional numbers in parentheses indicate the median numbers of 30 randomly measured diameter.

voltage (B), and distance between spinneret and collector (C), respectively.

The relations between the response variables (Y: enzymatic activity and diameter of fiber) and the input control factors (X: the electrospinning parameters) are shown in the response surfaces. In addition, statistical analysis of the response surface results obtained from response surface methodology (RSM) was performed using the central composite design (CCD) software mentioned above.

Fiber Characterization. The morphology and diameter of the produced fibers were analyzed by a scanning electron microscope (JEOL JSM-7800F, Thermal Field Emission Scanning Electron Microscope). The average diameter of the fiber was determined by manually measuring the diameter of 30 independent randomly selected fibers in different parts of the SEM image using ImageJ software (NIH). The types of functional groups in the fibers were analyzed by Fourier transform infrared (FTIR) spectrometry (Bruker Optik, Ettlingen, Germany) over 8 scans in a range 650−4000 cm^{-1}.

The changes in thermal properties of PVA fiber mats as a result of enzyme loading and cross-linking were analyzed using differential scanning calorimetry (DSC, Mettler-Toledo, Switzerland). DSC analysis was performed in a N_2 gas-filled chamber with a constant flow rate of 50 cm^3 min^{-1} and a heating/cooling rate of 20 °C min^{-1} in the range of 25 to 250 °C.

β-Glucosidase Activity Assay. The β-glucosidase activity of fibers shown in Table 1 was determined by measuring the amount of *p*-nitrophenol (*p*NP; Sigma-Aldrich) generated from the hydrolysis of 2.5 mg/mL of *p*-nitrophenyl-β-D-glucopyranoside (*p*NPG; Sigma-Aldrich) in citrate-phosphate buffer with pH and temperature settings according to the specified assay conditions. Specifically, each of the free forms of *Db*Exg1 and *Db*Exg1/PVA fibers was immersed in 500 μL of *p*NPG and placed in a dry bath incubator for 1 h. The reaction was stopped by removing the fibers followed by the addition of 500 μL of 0.5 M Na_2CO_3. The absorbance of the samples was analyzed using a UV−vis spectrophotometer at a wavelength of 405 nm and calibrated using *p*NP standard curves. One unit (U) of enzyme activity was defined as the formation of 1 μmole of *p*NP or S I per minute (if the amount of S I was quantitated).

Bradford Protein Assay. The amount of protein released from the enzyme/PVA fibers in the cross-linking solution was estimated. After immersing fibers in the solutions for 10 min, 100 μL aliquots were transferred and mixed with 100 μL of Coomassie blue dye (CB Protein Assay reagent, G-Biosciences, U.S.A.). The mixture was incubated for 5 min. The optical density of the final mixture was read at a wavelength of 595 nm. The absorbance of average test samples was subtracted from the absorbance of average blank samples before calibration using bovine serum albumin (BSA) standards. The final protein concentration results of the solution were expressed in μg/mL.

Quantitation of mogrosides using UPLC MS/MS. Mogroside standards (mogroside V, isomogroside V, siamenoside I, mogroside IV, and mogroside III E) were obtained from Chengdu Biopurify Phytochemicals Ltd. (Chengdu, China), and the calibration range was 50−1000 ng/mL. The system included a Waters Acquity UPLC equipped with a pump, column compartment, and autosampler, as well as a Waters TQS mass spectrometer (Waters, Milford, MA, USA) operated in positive electrospray ion (ESI^+) mode. An Acquity UPLC BEH C18 column (130 Å, 1.7 μm, 2.1 mm × 100 mm) was employed and maintained at 35 °C with a flow rate of 0.3 mL/min and injected with 2 μL of sample. The mobile phase consisted of 5% (A) and 100% methanol (B), both containing 0.01% formic acid. The linear gradient conditions were 45% B (0−1 min), 45−60% B (1−6 min), 60−99% B (6−6.2 min), 99% B (6.2−7 min), 99−45% B (7−8 min), and 45% B (8−10 min). The ESI parameters were set as follows: the capillary voltage was 3.1 kV, cone voltage was 38 V, desolvation temperature was 250 °C, source temperature was 150 °C, desolvation gas flow was 800 L/h, cone gas flow was 150 L/h, and nebulizer gas flow was 7.0 bar. The ESI scan range was set from m/z 50 to 1500 Da. All MS/MS data for the analytes were collected by multiple reaction monitoring (MRM) mode and MassLynx4.1 software. The optimized MRM conditions are shown in Table S2.

Statistical Analysis. All experiments were performed at least in triplicate. For the enzymatic activity and total protein analyses, all data were expressed as the means ± SD. Statistical analysis was performed using one-way ANOVA followed by Duncan's new multiple range test (SPSS for Windows, version 25.0.0.0). A value of $p < 0.05$ was considered to be statistically significant.

RESULTS AND DISCUSSION

Confirmation of MG V Conversion to S I by *S. cerevisiae exg1Δ::DbEXG1*. The *Db*Exg1 enzyme from *D. bruxellensis* has been found to have S I production specificity from MG V.[14] Nevertheless, the slow growth rate of this organism and its role in wine spoilage have hampered the production of S I through bioconversion.[14] Another kind of yeast, *S. cerevisiae*, with a rather short doubling time, effectively

https://dx.doi.org/10.1021/acs.jafc.0c02513
J. Agric. Food Chem. 2020, 68, 11790−11801

secretes *Sc*Exg1, which converts MG V into S I and MG IV as intermediates and MG III E as the end product.[13] Therefore, to produce *Db*Exg1 more effectively for S I production, the gene of *Db*Exg1 (*DbEXG1*) was incorporated into the chromosome of *S. cerevisiae* which to replace the original *Sc*Exg1 controlled under the *Sc*Exg1 enzyme promoter (Figures S1 and S2). The self-constructed *Db*Exg1-producing cells (*S. cerevisiae exg1*Δ::*DbEXG1*) were introduced to the S I conversion test. On the basis of the TLC results, it is quite obvious that S I was produced during the bioconversion process (Figure 1B), while the control group, *S. cerevisiae* BY4741 WT cells, first converted MG V to S I and MG IV as intermediates before proceeding to the final production of MG III E (Figure 1C). These results were similar to those of a previous study.[14]

Determination of *Db*Exg1 Loading Capacity in Fibers. When using fibers as a carrier for enzyme immobilization, the best outcome is to load the fibers with high amounts of enzymes while maintaining the fiber morphology.[22] Here, we first tried to determine how many enzymes could be mixed into the material while maintaining the fiber morphology. Through the preparation of PVA solutions with different enzyme loading percentages (4, 5, 6, and 7% w/v) for electrospinning, we found that the Taylor cone was not able to form once the enzyme content increased to 8% (w/v). Therefore, we decreased the amount of enzymes to 4∼7% (w/v). The SEM results in Figure 2 show that all fibers had a smooth and bead-free morphology, indicating synergy between the carrier PVA fibers and the *Db*Exg1 enzyme during the fiber fabrication process. Indeed, the diameter of the fiber also increased with increasing enzyme loading, suggesting the homogeneous dispersion of enzymes in PVA and the strong intermolecular interactions between the proteins and PVA.[17,22]

Meanwhile, a significantly lower enzymatic activity was observed in fibers with 4% enzyme loading compared to those with 5% and 7% enzyme loading. However, fibers with 4% and 6% of enzyme loading had a similar enzymatic activity (Figure 3A). These results demonstrate that the increase in enzyme loading was enough to produce fibers with acceptable enzymatic activity.

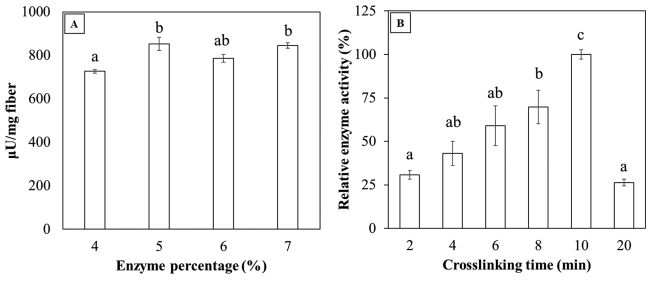

Figure 3. (A) Enzymatic activity tests of PVA fibers loaded with different percentages of enzymes. (B) The effect of cross-linking time on the catalytic activities of PVA fibers with 5% enzyme. Bars that do not share similar letters denote statistical significance ($p < 0.05$). The data were analyzed by one-way ANOVA followed by Duncan's multiple test.

loading tends to increase fiber catalytic activity. However, we did notice that the fibers had a maximum overall catalytic activity in high enzyme-loaded fibers. Further increasing of the enzyme loading results in an increased fiber diameter (Figure 2), which we believe will offset the enzymatic activity of fibers because of the decreased mass transfer efficiency in large fibers.[22,23,27,28] Therefore, we proposed that 5% enzyme

After determining the enzyme amount to be incorporated in the fibers, the cross-linking conditions of the fibers were established. From our results shown in Figure 3B, we suggest that an adequate cross-linking procedure involves the extension of the cross-linking time to prevent the disintegration of PVA fibers and to retain the enzymatic activity of the fibers. These results agree with the literature.[22] As such, 10 min was chosen as the appropriate cross-linking time for the enzyme/PVA fibers. However, 20 min of cross-linking results in lower fiber enzymatic activity.

Characterization of Enzyme/PVA Fibers. FTIR analysis was performed to confirm the presence of enzymes (*Db*Exg1) in PVA fibers as well as to investigate the interactions among PVA, *Db*Exg1, and phenylboronic acid (the cross-linker). All fibers shown in Figure 4 have a specific peak at 2939 cm^{-1},

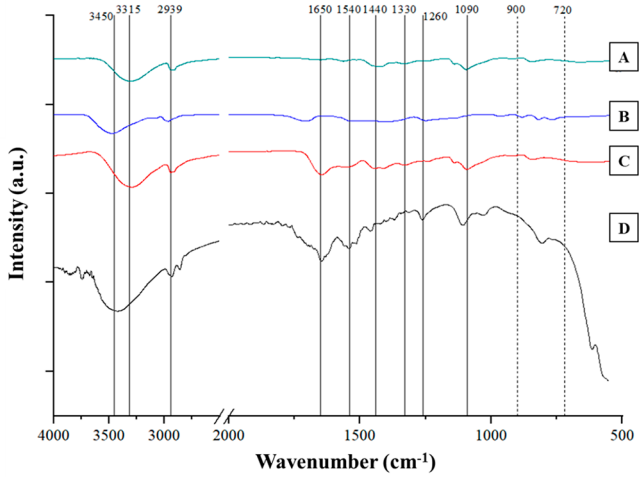

Figure 4. FT−IR spectra of (A) PVA fibers, (B) cross-linked PVA fibers, (C)*Db*Exg1/PVA fibers, and (D) cross-linked *Db*Exg1/PVA fibers.

which was characterized as the C−H group of PVA.[30] In the spectra of the noncrosslinked PVA and *Db*Exg1/PVA fibers depicted in Figure 4A and C, the observed peaks at 1090 and 1330 cm^{-1} represent stretching vibrations of C−O and $-CH_2$, respectively.[27,31] The specific peak at 1440 cm^{-1} indicates C−C stretching vibrations, and a broad stretching band at approximately 3315 cm^{-1} are associated with the −OH groups of PVA.[22] Meanwhile, a slight shift of peaks from 3315 to 3450 cm^{-1} in the cross-linked PVA and *Db*Exg1/PVA fibers (Figure 4B and D) might be caused by a diol complexation reaction through covalent boronate ester bonds occurred between two −OH groups of PVA and one phenylboronic acid ion during the cross-linking process. The diol complexation reaction also affect the overall structure of PVA which was indicated by the disappearance of peaks at 1090, 1330, and 1440 cm^{-1} that resemble the C−O, $-CH_2$, and C−C groups of PVA for all cross-linked fibers.[23,32]

The vibrations caused by out-of-plane C−H deformations in the monosubstituted aromatic ring of phenylboronic acid were manifested by the presence of peaks within the range of 900−720 cm^{-1}.[33] Furthermore, the stretching vibrations of B−O at 1260 cm^{-1} resulted from the diol complexation reaction between B−OH groups of phenylboronic acid and −OH

https://dx.doi.org/10.1021/acs.jafc.0c02513
J. Agric. Food Chem. 2020, 68, 11790−11801

groups of PVA, verifying the cross-linking of PVA and *Db*Exg1/PVA fibers using phenylboronic acid (Figure 4B and D).[34,35]

The presence of *Db*Exg1 was proven by an absorbance peak appearing at 1650 cm^{-1} in both cross-linked and non-crosslinked *Db*Exg1/PVA fibers (Figure 4C and D), which corresponded to the C═O stretching vibrations around the amide I region.[27,36,37] Although a slight shift of 1650 cm^{-1} signal was found in the IR curve of cross-linked *Db*Exg1/PVA fibers, which indicated structural changes of enzymes compared to the noncrosslinked fibers,[38] it is still an inevitable and a compromised procedure to prevent the PVA based fiber mat from disintegration when immersed into solutions. Also, the wider stretching bands at 3315 and 3450 cm^{-1} for fibers loaded with enzymes were due to the superposition of the stretching vibrations of O−H and N−H bonds, respectively.[28,37]

Further evidence indicating the presence of PVA in fibers was that the melting temperature appeared at 225.5 °C (Figure S3E). This result agrees with the literature value.[39] The cross-linking agent used in this study contains boron, which readily accepts a pair of electrons from the hydroxyl oxygen groups of PVA. This interaction leads to disruption of the crystallinity of PVA fibers due to the decreased electron density of hydroxyl oxygen groups and resulted in the disappearance of the melting temperature (Figure S3D). The change in the melting temperature of each fiber with different treatments is shown in Figure S3.

Relationship between the Enzymatic Activity and the Diameter of Produced Fibers. Here, we found that thicker fibers resulted in higher fiber enzymatic activity (Figures 2 and 3B). These results contradict the general idea that fibers with smaller diameters provide a large surface-to-volume ratio, giving higher enzymatic activity than that of large fibers. In this discovery, we refer our results to the existing experiential evidence from Wang and Hsieh,[17] where small fibers offer little accommodation space and dispersion areas for enzyme molecules, which lead to weaker polar intermolecular interactions. As a result, the enzymes could more easily detach from the fibers during cross-linking.

To further extend our aforementioned discoveries and results, we performed a protein leakage test on fibers of different diameters in solutions containing the cross-linking agent phenylboronic acid. As expected, the results shown in Table 2 revealed the inability of small-diameter fibers to retain enzymes within the fiber matrix, as more proteins were detected in the phenylboronic acid solution than when thicker fibers were used. Therefore, we suggest that large-diameter fibers are required to provide stronger intermolecular polar interactions between PVA and the enzyme to prevent enzyme leakage during the cross-linking process. For this reason, we aimed to optimize the combination of parameters used in the electrospinning process and to produce fibers with relatively large diameters. Additionally, the relationships between the diameter and the enzymatic activity of individual fibers were investigated again to determine their correlations.

Table 2. Protein Concentrations in the Crosslinking Solution of Fibers with Different Diameters

run[a]	enzymatic activity (μU/mg)	diameter (nm)	protein concentration (μg/mL)
19	32.27 ± 1.68[b]	201	16.22 ± 2.50[b]
13	47.07 ± 12.76[b]	245	10.89 ± 2.00[b]
20	239.11 ± 42.24[b]	294	9.33 ± 1.20[b]
8	243.65 ± 10.83[b]	343	5.11 ± 2.14[b]

[a]Electrospinning parameters for each run displayed in Table 1. [b]indicate that values within the same column are significantly different ($P < 0.05$). The data were analyzed by one-way ANOVA followed by Duncan's multiple tests.

Optimization of Electrospinning Parameters Using CCD-RSM. In this part of the experiment, we optimized three essential parameters in electrospinning, namely, (*A*) flow rate, (*B*) applied voltage, and (*C*) distance between spinneret and collector, to generate fibers with different diameters. In addition, we were interested in how those parameters affect the enzyme activity since the fiber diameter played a major role in determining the enzyme activity of the fibers. The fiber diameter and enzyme activity data, which were acquired from experiments based on the central composite design (CCD), are shown in Table 1. According to the data fitting summary, the cubic model and the full quadratic polynomial model were selected as model equations to predict the enzymatic activity (3) and fiber diameter (4) of the produced fibers, respectively. These coded equations are as follows:

$$Y = 210.37 + 34.67A - 12.82B - 57.75C + 0.64AB - 18.39AC + 30.82BC - 6.55A^2 - 26.12B^2 - 27.60C^2 - 17.18ABC + 10.30A^2B - 8.66A^2C - 22.26AB^2 \quad (3)$$

$$Y = 244.42 + 16.60A - 9.36B - 30.56C - 6.75AB - 12.75AC + 3.75BC + 24.50A^2 + 14.83B^2 - 6.83C^2 \quad (4)$$

The results of the analysis of variance (ANOVA) shown in Table 3 revealed that variables *A*, *B*, *C*, *AC*, *BC*, A^2, B^2, C^2, *ABC*, and AB^2 significantly influenced the enzymatic activity of fibers ($p < 0.05$). Meanwhile, the lack-of-fit test, which is an evaluation to determine the impact of discrepancies between the actual and predicted values on the pure error among replicates, had a value of 0.1962, which was higher than 0.05, i.e., not significant (p-value <0.05). In addition, the lack-of-fit *F*-value of 2.22 implies that the lack of fit is not significant. There is a 19.62% chance that a lack-of-fit *F*-value this large could occur due to noise. Therefore, the cubic model adequately explains the interactions of parameters in the region of experimentation. The goodness of fit of the proposed model for enzyme activity predictions was also determined. Figure 5A−D show enzyme activity values located in a narrow range of normal probability lines, diagonal lines, and two zero-axes, suggesting the adequacy of the model used to predict the experimental results.

The ANOVA (Table 4) shows the diameter of the produced fibers, which were sensitive to all the variations of independent variables (*A*, *B*, and *C*), one interactive cross-product coefficient (*AC*), and two quadratic term coefficients (A^2 and B^2), with $p < 0.05$. In addition, a lack-of-fit *p*-value larger than 0.05 indicates the success of the RSM model in predicting the variance in the test and the experimental data. The scattering of diameter values in Figure 5E−H also describes the fitness of the model.

From the response surface plot depicted in Figure 6A and B, we can see that a higher flow resulted in a higher enzymatic activity of fibers. In addition, the sharp curvature of the curve in Figure 6C shows the reciprocal relationships between the distance and enzymatic activity of the fibers. Meanwhile, the optimum value of applied voltage as the driving force to stretch the feed solution worked synergistically with the flow rate and

https://dx.doi.org/10.1021/acs.jafc.0c02513
J. Agric. Food Chem. 2020, 68, 11790−11801

Table 3. Analysis of Variance (ANOVA) for Enzymatic Activity as the Response[a,b]

source	sum of squares	df	mean square	*F*-value	*p*-value	
model	92784.44	13	7137.26	111.29	<0.0001	significant
A, flow rate	5409.04	1	5409.04	84.34	<0.0001	
B, voltage	840.91	1	840.91	13.11	0.0111	
C, distance	18823.82	1	18823.82	293.52	<0.0001	
AB	3.28	1	3.28	0.0512	0.8285	
AC	2706.11	1	2706.11	42.20	0.0006	
BC	7601.18	1	7601.18	118.53	<0.0001	
A^2	441.76	1	441.76	6.89	0.0393	
B^2	8479.62	1	8479.62	132.22	<0.0001	
C^2	11065.68	1	11065.68	172.55	<0.0001	
ABC	2362.44	1	2362.44	36.84	0.0009	
A^2B	330.89	1	330.89	5.16	0.0635	
A^2C	247.98	1	247.98	3.87	0.0968	
AB^2	1427.31	1	1427.31	22.26	0.0033	
residual	384.78	6	64.13			
lack of fit	118.39	1	118.39	2.22	0.1962	not significant
pure error	266.40	5	53.28			
cor total	93169.22	19				

[a] R^2: 0.9959, Adj. R^2: 9869, Pred. R^2: 0.6825, Std. Dev. = 8.01, CV = 4.70%, PRESS = 29 578.50. [b] $p < 0.05$ indicates that the model terms are significant.

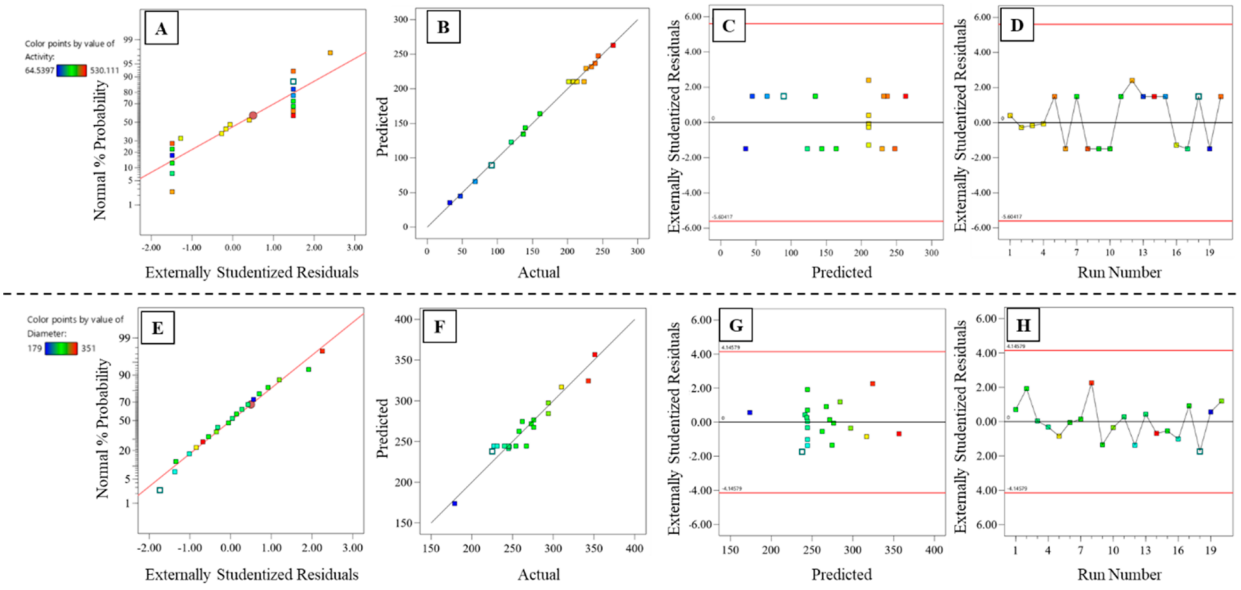

Figure 5. Diagnostic plots for the enzymatic activity (upper panel) and diameter (lower panel) of fibers: (A, E) normal probability plot on a probit scale, (B, F) predicted versus actual values plot, (C, G) studentized residuals versus predicted values plot, and (D, H) studentized residuals versus run number plot.

distance to promote the production of fibers with the highest enzymatic activity (Figure 6A and C).

The delineated response surface plots depicted in Figure 6D and E showed little change in the diameter when the flow rate was set between 0.004 and 0.006 mL/min, and the diameter started to increase to the highest level when the flow rate increased to 0.007−0.008 mL/min. The increased flow rate resulted in an increased feeding rate at the tip of the spinneret, creating conditions favoring the movement of materials and forming thicker fibers. Additionally, it can be observed from Figure 6D and F that changes in the applied voltage had little effect on the fiber diameter, while Figure 6E and F shows that a decrease in the distance between the spinneret and collector resulted in a linear increase in the fiber diameter.

From the overall CCD-RSM results shown in Table 1, we again proved that fibers with large diameters resulted in higher enzymatic activity and that all the tested parameters had similar trends regarding the fiber diameter and enzymatic activity (Figure 6). However, we found that fibers produced from both the 8th and 14th runs with a relatively high flow rate and short distance had significantly high values of enzymatic activity as well as diameter. The instability of the electrospinning process caused by the unsuitable parameter combinations in the 14th run resulted in fibers with a nonhomogeneous morphology (Figure S4A). Meanwhile, the spinning condition for the 8th run generated fibers with a smooth and bead-free morphology (Figure S4B). Considering the information regarding the fiber homogeneity and enzymatic activity, we ultimately chose the parameters of the

https://dx.doi.org/10.1021/acs.jafc.0c02513
J. Agric. Food Chem. 2020, 68, 11790−11801

Table 4. Analysis of Variance (ANOVA) for Diameter as the Response[a,b]

source	sum of squares	df	mean square	*F*-value	*p*-value	
model	28 957.99	9	3217.55	15.33	<0.0001	significant
A, flow rate	3444.50	1	3444.50	16.41	0.0023	
B, voltage	1149.38	1	1149.38	5.48	0.0413	
C, distance	12 741.53	1	12 741.53	60.70	<0.0001	
AB	364.50	1	364.50	1.74	0.2170	
AC	1300.50	1	1300.50	6.20	0.0320	
BC	112.50	1	112.50	0.5359	0.4809	
A^2	6173.68	1	6173.68	29.41	0.0003	
B^2	2735.72	1	2735.72	13.03	0.0048	
C^2	677.93	1	677.93	3.23	0.1025	
residual	2099.21	10	209.92			
lack of fit	995.21	5	199.04	0.9015	0.5439	not significant
pure error	1104.00	5	220.80			
cor total	31057.20	19				

[a] R^2: 0.9324, Adj. R^2: 0.8716, Pred. R^2: 0.7235, Std. Dev. = 14.49, CV = 5.47%, PRESS = 8586.84. [b] $p < 0.05$ indicates that the model terms are significant.

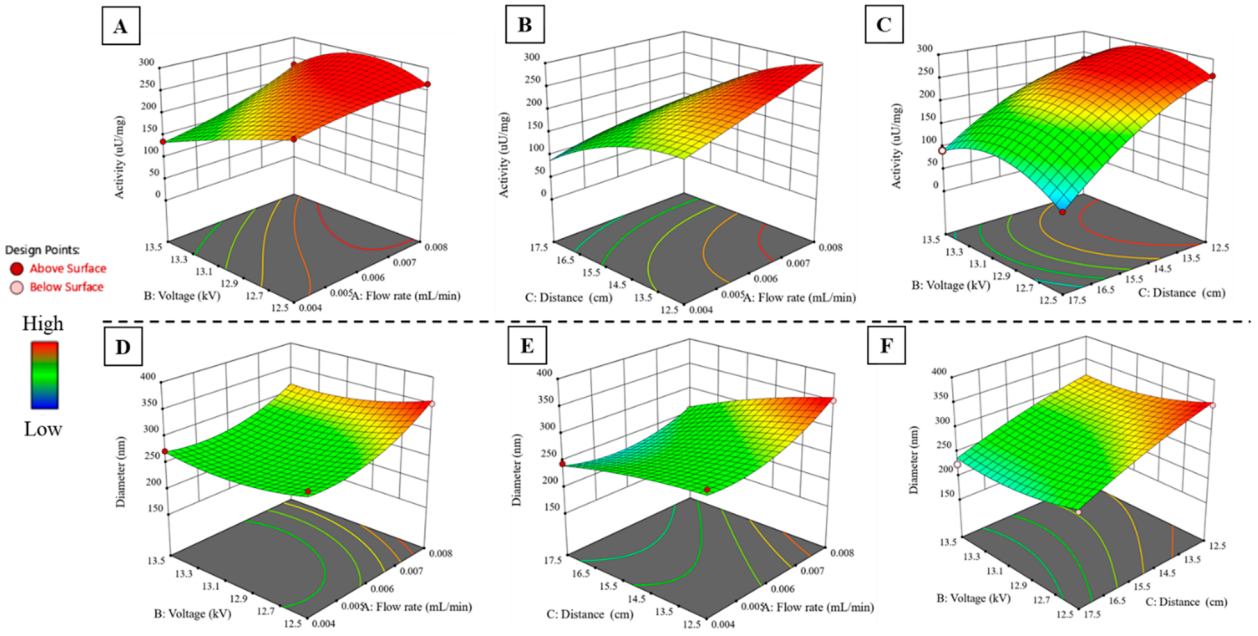

Figure 6. Response surface and contour plots for the mutual effects of parameters: (A, D) voltage and flow rate, (B, E) flow rate and distance, and (C, F) voltage and distance on enzymatic activity (upper panel) and diameter (lower panel) of fibers.

8th run as the optimum electrospinning parameters (0.009 mL/min, 13.0 kV, and 15.0 cm) for fiber fabrication.

Characterization of Enzyme Fiber Working Conditions. The optimum pH working conditions for the enzyme fibers were assessed within the pH range from 3.0 to 9.0 at 50 °C. From Figure 7A, we observed that immobilization did not change the optimum pH of the enzyme but allowed a greater enzymatic activity to be maintained than that of the free enzyme at pH 4 and 6.

Figure 7B shows the enzyme reactivity of fibers at different temperatures from 30 to 80 °C at pH 5.0. Note that there was no significant difference in the relative activity between immobilized and free enzymes at a reaction temperature above 50 °C; this is because *Db*Exg1 was very sensitive to high temperatures and easily became denatured once incubated at temperatures that exceeded its optimum limit.[18] In addition, we realized that immobilization would cause a decrease in the free enzyme activity when the reaction temperature was set under an optimum working temperature of 50 °C. This result was most likely due to the increased intermolecular interactions of enzymes and the PVA matrix, acting as a physical barrier that inhibited the substrate-enzyme interactions under this less triggering condition.[35] This is also the case because intermolecular interactions decrease the flexibility of the enzyme within PVA molecules that further protect the enzyme under more extreme pH conditions.[22,23]

The thermal stability test of the free enzyme and immobilized enzyme fibers at 60 °C provided additional evidence showing that PVA molecules maintain the stability of the enzyme. The results given in Figure 7C indeed confirm the temperature sensitivity of the enzyme, where extreme losses of enzyme activity occurred during the first 10 min of incubation. However, compared to the free enzyme, the immobilized enzyme was able to maintain a significantly higher catalytic performance during extended 50 min heat exposure. These results were also observed in a previous study.[24]

https://dx.doi.org/10.1021/acs.jafc.0c02513
J. Agric. Food Chem. 2020, 68, 11790−11801

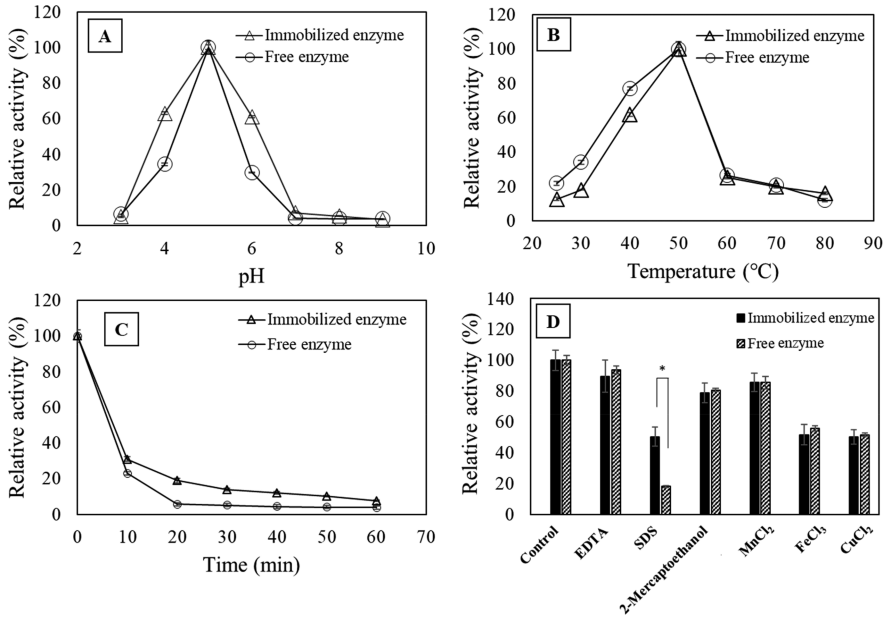

Figure 7. Relative activity of free and immobilized enzymes under different (A) pH values and (B) temperatures when incubated at 50 °C for 1 h and pH 5.0 for 1 h, respectively. (C) The thermostability of free and immobilized enzymes tested at 60 °C and pH 5.0 for 1 h. (D) Effects of chemical agents and metal ions (10 mM) on the relative activity of free and immobilized enzymes. * Indicates significantly different results from the indicated groups by Student's *t* test with *p*-value <0.05.

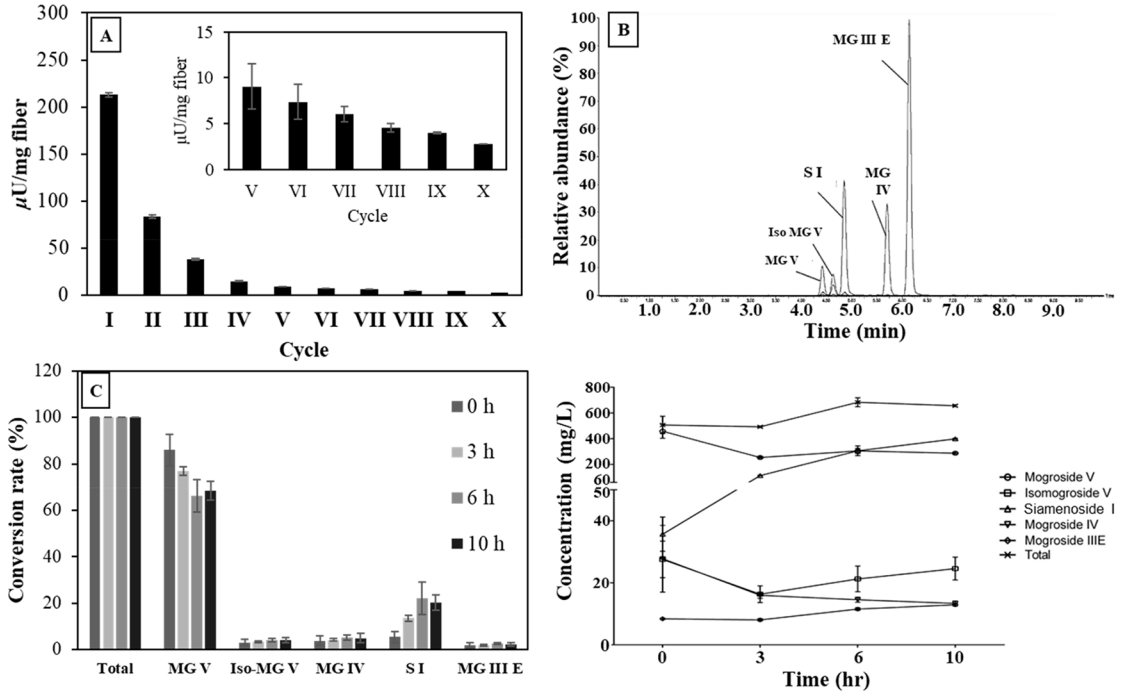

Figure 8. Substrate conversion activity of cross-linked enzyme/PVA fibers. (A) *p*NPG conversion activities during 10 cycles of reuse. (B) A representative mogroside distribution analyzed by UPLC−MS/MS. (C) Time course of the mogroside conversion rate and mogroside content under conditions of 50 °C at pH 5.

Enzymes used in food industries may have the chance to come into contact with chemicals that influence their activity. For example, chemicals including metal ions present in water or from equipment corrosion can work as either activators or inhibitors of enzymes. Meanwhile, chemicals used in the cleaning of equipment, such as detergents, can also damage the tertiary structure of enzymes and lead to decreased enzyme activity. Therefore, several metal ions that have been reported to be inhibitors of *β*-glucosidase ($MnCl_2$, $FeCl_3$, and $CuCl_2$), as well as other chemicals (EDTA, SDS, and 2-mercaptoethanol) within a concentration of 10 mM, were subjected to a buffer enzymatic activity test to evaluate their influence on the enzymatic activity.[40] The results in Figure 7D show all the metal ions tested in this study had the same level of inhibition toward the enzymatic activity of both free and immobilized enzymes. Similar results were also observed for EDTA and 2-

https://dx.doi.org/10.1021/acs.jafc.0c02513
J. Agric. Food Chem. 2020, 68, 11790−11801

mercaptoethanol. However, enzymes in fibers were less sensitive than free enzymes toward SDS treatment. These results suggested that the fiber matrices can protect the enzyme hydrophobic segments from being denatured by detergents such as SDS and thus preserve the activity.

Mogroside Conversion Rate Test in Fibers. First, the enzymatic activity of the fibers was evaluated for several cycles of reuse via the *p*NPG conversion mentioned previously, but the fibers were rinsed with water before transferring to the next cycle. By measuring the remaining *p*NPG conversion activity in the fibers after each of the 1-h reaction cycles, we showed that the fibers displayed high enzymatic activity in the first cycle, which was 213.25 ± 8.25 μU per mg of fiber, and that this activity decreased along with the reuse cycles (Figure 8A). The average enzymatic activity toward *p*NPG during those 10 cycles of usage was 38.25 ± 3.14 μU per mg of fiber. We think that the decrease in enzyme activity in fibers might be caused by the leakage of enzymes or the increase of inaccessibility of the enzyme's active sites toward the substrates due to fiber swelling. Nevertheless, the immobilized enzyme retained approximately 10% of its initial activity after four cycles of reuse, which offers potential for continuous use of the immobilized enzyme in industrial applications.[27]

The ability of fibers to convert MG V into S I was confirmed by incubating 90 mg of a produced fiber mat in 5 mL of monk fruit extract containing 80% MG V for 0, 3, 6, and 10 h at the optimum reaction conditions (citrate-phosphate buffer pH 5.0, 50 °C). UPLC−MS analysis was conducted to quantify the amount of each mogroside (Figure 8B). The overall results show that the amount of MG V gradually decreased from 80% to 60% of the total MGs after 10 h of incubation, while a significant increase in the amount of S I from 5% to 22% of the total MGs was observed (Figure 8C left). In addition, there were no significant changes in the other types of MGs including iso-MG V, MG IV, and MG III E, suggesting a highly specific S I conversion activity of the cross-linked enzyme/PVA fiber (Figure 8C left). An S I production rate of approximately 118 ± 0.08 mg L^{-1} h^{-1} per gram of fiber was calculated based on a 5 mL-chamber setting which contains 90 mg of fiber and a net S I production amount of 106.11 g/mL within 10 h (Figure 8C right). Besides, the average enzymatic activity toward S I production was 11.48 ± 0.48 μU per mg of fiber.

Since batch studies were performed in the MG conversion tests for 10 h, it is likely that the enzymes previously thought to detach from the fiber matrix should still contribute to the MG V conversion in this enclosed 5 mL-chamber system. However, the conversion rate of S I gradually decreased and reached a plateau after 10 h of reaction. We suggest that there was minimal enzyme leakage in the fiber scaffold; otherwise, the amount of S I would continue to go upward as the activity of the free enzyme remains. Hence, the saturated S I conversion result shown in this study was more related to the inaccessibility of the enzyme's active sites toward the substrates, which was caused by the excessive swelling of the hydrophilic PVA fibers in aqueous solutions and a growing diffusion resistance of the fiber.[41] In other words, a decrease in the fiber enzymatic activity toward *p*NPG in each cycle was caused mainly by the aforementioned swelling of fibrous morphology after several reuses and not by the cause of enzyme leakage of fibers although data on enzyme leakage kinetics. Nevertheless, the ability of the cross-linked enzyme/PVA fibers to be used repeatedly proved their potential for utilization in continuous and larger-scale S I production as long as the swelling can be properly controlled.

In summary, since we calculated the production rate of S I, we can increase the amount of S I production by increasing the operating time, scale, and fiber density in future studies. Accordingly, in this study, the overall illustration of *Db*Exg1 immobilization using electrospinning certainly presents new insights to overcome the stability and reusability issues encountered in the application of these enzymes to sustainably redistribute mogrosides for use as natural sweeteners.

■ ASSOCIATED CONTENT

Supporting Information

The Supporting Information is available free of charge at https://pubs.acs.org/doi/10.1021/acs.jafc.0c02513.

Table S1, sequence of primers used in this study; Table S2, optimized MRM transition and parameters for 5 mogrosides; Figure S1, conceptual schematic showing the inverse PCR procedure; Figure S2, screening of yeast transformants with *exg1*Δ*::KanMX4* replaced with the *Db*Exg1-*URA3* cassette; Figure S3, DSC curves of the PVA and enzyme/PVA fibers with/without chemical cross-linking; and Figure S4, SEM micrographs of enzyme/PVA fibers produced in the 14th and 8th runs in the CCD table (PDF)

■ AUTHOR INFORMATION

Corresponding Author

Reuben Wang − *Institute of Food Safety and Health, College of Public Health and Master of Public Health Program, College of Public Health, National Taiwan University, Taipei City, Taiwan; Department of Food Science, College of Agriculture, Tunghai University, Taichung City, Taiwan;* orcid.org/0000-0002-6328-7331; Phone: +886-2-33668084; Email: reubenwang@ntu.edu.tw; Fax: +886-2-33668114

Authors

Virly − *Department of Food Science, College of Agriculture, Tunghai University, Taichung City, Taiwan*

Chun-Hui Chiu − *Graduate Institute of Health Industry and Technology, Research Center for Chinese Herbal Medicine and Research Center for Food and Cosmetic Safety, College of Human Ecology, Chang Gung University of Science and Technology, Taoyuan City, Taiwan; Department of Traditional Chinese Medicine, Chang Gung Memorial Hospital, Keelung City, Taiwan*

Tsan-Yu Tsai − *Institute of Polymer Science and Engineering, National Taiwan University, Taipei City, Taiwan*

Yi-Cheun Yeh − *Institute of Polymer Science and Engineering, National Taiwan University, Taipei City, Taiwan*

Complete contact information is available at: https://pubs.acs.org/10.1021/acs.jafc.0c02513

Author Contributions

▽These authors contributed equally to this work.

Funding

This work is supported by the Ministry of Science and Technology (MOST), Republic of China (Grant No. 106-2218-E-029-002-MY2 and 107-2113-M-002-025-MY4) and Chang Gung University of Science and Technology (ZRRPF3J0071).

Notes

The authors declare no competing financial interest.

■ ACKNOWLEDGMENTS

We thank Dr. Wen-Hsin Chung for technical assistance with the SEM analysis.

■ REFERENCES

(1) Lee, C.-h. Intense sweetener from Lo Han Kuo (*Momordica grosvenori*). *Experientia* **1975**, *31*, 533−534.
(2) Matsumoto, K.; Kasai, R.; Ohtani, K.; Tanaka, O. Minor cucurbitane-glycosides from fruits of *Siraitia grosvenori* (Cucurbitaceae). *Chem. Pharm. Bull.* **1990**, *38*, 2030−2032.
(3) Cho, S., Determination of the generally recognized as safe (GRAS) status of *Siraitia grosvenori* Swingle (Luo Han Guo) fruit extract as a food ingredient. 2017, pp 1−140.
(4) Takemoto, T.; Arihara, S.; Nakajima, T.; Okuhira, M. Studies on the constituents of Fructus momordicae. II. Structure of sapogenin. *Yakugaku Zasshi* **1983**, *103*, 1155−1166.
(5) Takemoto, T.; Arihara, S.; Nakajima, T.; Okuhira, M. Studies on the constituents of Fructus momordicae. I. on the sweet principle. *Yakugaku Zasshi* **1983**, *103*, 1151−1154.
(6) Takemoto, T.; Arihara, S.; Nakajima, T.; Okuhira, M. Studies on the constituents of Fructus momordicae. III. structure of mogrosides. *Yakugaku Zasshi* **1983**, *103*, 1167−1173.
(7) Jia, Z.; Yang, X. A minor, sweet cucurbitane glycoside from *Siratia grosvenorii*. *Nat. Prod. Commun.* **2009**, *4*, 769−772.
(8) Qiao, J.; Luo, Z.; Gu, Z.; Zhang, Y.; Zhang, X.; Ma, X. Identification of a Novel Specific Cucurbitadienol Synthase Allele in *Siraitia grosvenorii* Correlates with High Catalytic Efficiency. *Molecules* **2019**, *24* (3), 627
(9) Tan, V. W. K.; Wee, M. S. M.; Tomic, O.; Forde, C. G. Temporal sweetness and side tastes profiles of 16 sweeteners using temporal check-all-that-apply (TCATA). *Food Res. Int.* **2019**, *121*, 39−47.
(10) Zhou, Y.; Amentrout, R. W.; Woodyer, R. D.; Bridges, J. R.; Schunk, T. C.; Fletcher, J. N. Redistribution of mogrol glycoside content (WO 2014/150127). 2014.
(11) Chen, X. B.; Zhuang, J. J.; Liu, J. H.; Lei, M.; Ma, L.; Chen, J.; Shen, X.; Hu, L. H. Potential AMPK activators of cucurbitane triterpenoids from *Siraitia grosvenorii* Swingle. *Bioorg. Med. Chem.* **2011**, *19*, 5776−5781.
(12) Murata, Y.; Ogawa, T.; Suzuki, Y. A.; Yoshikawa, S.; Inui, H.; Sugiura, M.; Nakano, Y. Digestion and absorption of *Siraitia grosvenori* triterpenoids in the rat. *Biosci., Biotechnol., Biochem.* **2010**, *74*, 673−676.
(13) Chiu, C.-h.; Wang, R.; Lee, C.-c.; Lo, Y.-c.; Lu, T.-j. Biotransformation of mogrosides from *Siraitia grosvenorii* Swingle by *Saccharomyces cerevisiae*. *J. Agric. Food Chem.* **2013**, *61*, 7127−7134.
(14) Wang, R.; Chen, Y.-c.; Lai, Y.-j.; Lu, T.-j.; Huang, S.-t.; Lo, Y.-C. *Dekkera bruxellensis*, a beer yeast that specifically bioconverts mogroside extracts into the intense natural sweetener siamenoside I. *Food Chem.* **2019**, *276*, 43−49.
(15) Chakraborty, S.; Asgeirsson, B.; Rao, B. J. A measure of the broad substrate specificity of enzymes based on 'duplicate' catalytic residues. *PLoS One* **2012**, *7* (11), e49313.
(16) Datta, S.; Christena, L. R.; Rajaram, Y. R. Enzyme immobilization: an overview on techniques and support materials. *3 Biotech* **2013**, *3* (1), 1−9.
(17) Yushkova, E. D.; Nazarova, E. A.; Matyuhina, A. V.; Noskova, A. O.; Shavronskaya, D. O.; Vinogradov, V. V.; Skvortsova, N. N.; Krivoshapkina, E. F. Application of Immobilized Enzymes in Food Industry. *J. Agric. Food Chem.* **2019**, *67* (42), 11553−11567.
(18) Jeong, D. W.; Hyeon, J. E.; Shin, S. K.; Han, S. O. Trienzymatic Complex System for Isomerization of Agar-Derived d-Galactose into d-Tagatose as a Low-Calorie Sweetener. *J. Agric. Food Chem.* **2020**, *68* (10), 3195−3202.
(19) Reneker, D. H.; Chun, I. Nanometre diameter fibres of polymer, produced by electrospinning. *Nanotechnology* **1996**, *7*, 216−223.
(20) Pillay, V.; Dott, C.; Choonara, Y. E.; Tyagi, C.; Tomar, L.; Kumar, P.; Du Toit, L. C.; Ndesendo, V. M. K. A review of the effect of processing variables on the fabrication of electrospun nanofibers for drug delivery applications. *J. Nanomater.* **2013**, *2013*, 1−22.
(21) Wen, P.; Wen, Y.; Zong, M.-H.; Linhardt, R. J.; Wu, H. Encapsulation of Bioactive Compound in Electrospun Fibers and Its Potential Application. *J. Agric. Food Chem.* **2017**, *65* (42), 9161−9179.
(22) Wang, Y.; Hsieh, Y. L. Immobilization of lipase enzyme in polyvinyl alcohol (PVA) nanofibrous membranes. *J. Membr. Sci.* **2008**, *309* (1), 73−81.
(23) Nunes, M. A. P.; Martins, S.; Rosa, M. E.; Gois, P. M. P.; Fernandes, P. C. B.; Ribeiro, M. H. L. Improved thermostable polyvinyl alcohol electrospun nanofibers with entangled naringinase used in a novel mini-packed bed reactor. *Bioresour. Technol.* **2016**, *213*, 208−215.
(24) İspirli Doğaç, Y.; Deveci, İ.; Mercimek, B.; Teke, M. A comparative study for lipase immobilization onto alginate based composite electrospun nanofibers with effective and enhanced stability. *Int. J. Biol. Macromol.* **2017**, *96*, 302−311.
(25) Dai, M.; Jin, S.; Nugen, S. Water-Soluble Electrospun Nanofibers as a Method for On-Chip Reagent Storage. *Biosensors* **2012**, *2*, 388−95.
(26) Aldhahri, M. M.; Almulaiky, Y. Q.; El-Shishtawy, R. M.; Al-Shawafi, W.; Alngadh, A.; Maghrabi, R. Facile Immobilization of Enzyme via Co-Electrospinning: A Simple Method for Enhancing Enzyme Reusability and Monitoring an Activity-Based Organic Semiconductor. *ACS Omega* **2018**, *3* (6), 6346−6350.
(27) Moreno-Cortez, I. E.; Romero-Garcia, J.; Gonzalez-Gonzalez, V.; Garcia-Gutierrez, D. I.; Garza-Navarro, M. A.; Cruz-Silva, R. Encapsulation and immobilization of papain in electrospun nanofibrous membranes of PVA cross-linked with glutaraldehyde vapor. *Mater. Sci. Eng., C* **2015**, *52*, 306−314.
(28) dos Santos, J. P.; Zavareze, E. d. R.; Dias, A. R. G.; Vanier, N. L. Immobilization of xylanase and xylanase − β-cyclodextrin complex in polyvinyl alcohol via electrospinning improves enzyme activity at a wide pH and temperature range. *Int. J. Biol. Macromol.* **2018**, *118*, 1676−1684.
(29) Wang, R.; Lin, P. Y.; Huang, S. T.; Chiu, C. H.; Lu, T. J.; Lo, Y. C. Hyperproduction of beta-Glucanase Exg1 Promotes the Bioconversion of Mogrosides in Saccharomyces cerevisiae Mutants Defective in Mannoprotein Deposition. *J. Agric. Food Chem.* **2015**, *63* (47), 10271−9.
(30) Wen, P.; Zhu, D.-H.; Wu, H.; Zong, M.-H.; Jing, Y.-R.; Han, S.-Y. Encapsulation of cinnamon essential oil in electrospun nanofibrous film for active food packaging. *Food Control* **2016**, *59*, 366−376.
(31) Alghunaim, N. S. Optimization and spectroscopic studies on carbon nanotubes/PVA nanocomposites. *Results Phys.* **2016**, *6*, 456−460.
(32) Nishiyabu, R.; Shimizu, A. Boronic acid as an efficient anchor group for surface modification of solid polyvinyl alcohol. *Chem. Commun.* **2016**, *52* (63), 9765−9768.
(33) Ermakova, E. N.; Sysoev, S. V.; Nikulina, L. D.; Tsyrendorzhieva, I. P.; Rakhlin, V. I.; Kosinova, M. L. Trimethyl-(phenyl)silane — a precursor for gas phase processes of SiC_x:H film deposition: Synthesis and characterization. *Modern Electronic Materials* **2015**, *1* (4), 114−119.
(34) Balachander, L.; Ramadevudu, G.; Shareefuddin, M.; Sayanna, R.; Venudhar, Y.C. IR analysis of borate glasses containing three alkali oxides. *ScienceAsia* **2013**, *39*, 278.
(35) Ravangave, L.; Devde, G. Structure and Physical Properties of $59B_2O_3-10Na_2O-(30-x)CdO-xZnO-1CuO$ $(0 \le x \le 30)$ Glass System. 2018.
(36) Barth, A. Infrared spectroscopy of proteins. *Biochim. Biophys. Acta, Bioenerg.* **2007**, *1767* (9), 1073−1101.

https://dx.doi.org/10.1021/acs.jafc.0c02513
J. Agric. Food Chem. 2020, 68, 11790−11801

(37) Shoba, E.; Lakra, R.; Kiran, M. S.; Korrapati, P. S. Design and development of papain − urea loaded PVA nanofibers for wound debridement. *RSC Adv.* **2014**, *4*, 60209−60215.
(38) Secundo, F. Conformational changes of enzymes upon immobilisation. *Chem. Soc. Rev.* **2013**, *42* (15), 6250−61.
(39) Lemma, S. M.; Scampicchio, M.; Mahon, P. J.; Sbarski, I.; Wang, J.; Kingshott, P. Controlled Release of Retinyl Acetate from β-Cyclodextrin Functionalized Poly (vinyl alcohol) Electrospun Nanofibers. *J. Agric. Food Chem.* **2015**, *63* (13), 3481−3488.
(40) Kuo, H.-P.; Wang, R.; Huang, C.-Y.; Lai, J.-T.; Lo, Y.-C.; Huang, S.-T. Characterization of an extracellular β-glucosidase from *Dekkera bruxellensis* for resveratrol production. *Journal of Food and Drug Analysis* **2018**, *26* (1), 163−171.
(41) Ariga, O.; Itoh, K.; Sano, Y.; Nagura, M. Encapsulation of Biocatalyst with PVA Capsules. *J. Ferment. Bioeng.* **1994**, *78* (1), 74−78.

https://dx.doi.org/10.1021/acs.jafc.0c02513
J. Agric. Food Chem. 2020, 68, 11790−11801